Title
SEARCH FOR AN ELECTRON MASS SHIFT IN 133Cs IN AN INTENSE ELECTROMAGNETIC FIELD

Author
Mowat, J. Richard

Publication Date
1969-08-15

UCRL-19245

cy. 2

SEARCH FOR AN ELECTRON MASS SHIFT IN ^{133}Cs IN AN INTENSE ELECTROMAGNETIC FIELD

J. Richard Mowat
(Ph. D. Thesis)

August 15, 1969

AEC Contract No. W-7405-eng-48

LAWRENCE RADIATION LABORATORY
UNIVERSITY of CALIFORNIA BERKELEY

cy. 2

UCRL-19245

DISCLAIMER

SEARCH FOR AN ELECTRON MASS SHIFT IN ^{133}Cs
IN AN INTENSE ELECTROMAGNETIC FIELD

Contents

SEARCH FOR AN ELECTRON MASS SHIFT IN ^{133}Cs IN AN INTENSE ELECTROMAGNETIC FIELD

J. Richard Mowat

Department of Physics
and
Lawrence Radiation Laboratory
University of California
Berkeley, California

August 15, 1969

ABSTRACT

The possibility that the mass of a bound electron changes when placed in an intense electromagnetic field has been investigated both theoretically and experimentally. The atomic-beam magnetic-resonance technique was used to examine hyperfine-structure shifts in ^{133}Cs that occur when the atom is subjected to an intense, non-resonant magnetic field perpendicular to the static "C" field. A 2921 MHz TM_{010} cavity was situated between Ramsey separated oscillatory loops, which induced the transitions of interest. Shifts were observed for six $\Delta F = \pm 1$, $\Delta m_F = \pm 1$ transitions at field-independent points. No evidence was found for an electron mass shift. Excellent agreement is found between all observed shifts and those expected from a multi-level Bloch-Siegert effect. Theoretical reasons, based upon perturbation theory, are given explaining why the mass-shift effect does not occur in the ground state hyperfine-structure of a hydrogen-like system.

I. INTRODUCTION

The atomic-beam magnetic-resonance technique was developed by Rabi[1] and his co-workers in the late 1930's to measure nuclear magnetic moments. Since then the method has proven extremely fruitful, yielding detailed knowledge of nuclear and atomic structure through precise measurements of nuclear spins and moments and atomic hyperfine-structure (hfs) energy separations. Alkali g_J values[2] and hfs separations $\Delta\nu$ measured by this technique to better than one part per million are some of the most accurately known of all physical quantities. Even so, these measurements do not exhaust the potential of the method.

Because of its inherent high precision, the atomic-beam magnetic-resonance technique has often been used for special studies of extremely small effects. In 1957, for example, Haun and Zacharias[3] used this method to measure the differential Stark shift of the ^{133}Cs ground state hfs, an effect so small that an electric field of 10^5 V/cm induces a shift of only 2-1/2 parts per million of the transition frequency. Lipworth and Sandars[4] have measured even smaller Stark shifts of ^{133}Cs ground-state Zeeman levels that amount to a little more than one part in 10^8 of the transition frequency for a 10^5 V/cm electric field. Tests of parity conservation and time-reversal invariance have been the object of very precise work, again using ^{133}Cs, to establish an upper limit to the electric dipole moment of the electron.[5] The cesium atom and the atomic-beam magnetic-resonance technique make a good combination for the study of very small perturbations within atomic systems.

In 1952 the Indian physicist Sengupta,[6] while studying the solutions to the Dirac equation for an electron in a plane wave field (Compton Scattering), first suggested the possibility that the mass of a free electron might be observed to increase when the electron is allowed to interact with an intense electromagnetic field. This mass-shift effect is just one of many interesting and controversial predictions of theories of intense-field electrodynamics that have appeared over the past few years. Sarachik[7] has recently made a comprehensive survey of these effects, none of which has yet been observed experimentally owing to the difficulty in generating sufficiently intense fields.

In 1966 Reiss[8] suggested that, under favorable conditions, an intensity-dependent mass shift could be observed for a bound electron. An electron mass increase would affect precision measurements made of spectral lines from a hydrogen-like system placed in an intense plane wave environment. Such spectral lines depend on the electron mass through the Rydberg energy

$$Ry = -\frac{1}{2}\alpha^2 mc^2$$

(where α is the Sommerfeld fine structure constant, and mc^2 is the electron rest energy), and through the Bohr magneton

$$\mu_o = \frac{e\hbar}{2mc} \quad .$$

Thus motivated, it was decided to investigate transition frequency shifts of the ^{133}Cs ground state hfs induced by the intense non-resonant fields in a microwave cavity. The mass-shift hypothesis for an electron bound in the ground state of a hydrogen-like system was examined in

detail both theoretically and experimentally. It was found that if all the effects of the field are treated in a consistent manner using perturbation theory, then the mass-shift effect does not occur. In addition, extensive experimental work of sufficient sensitivity to observe the mass-shift effect has yielded negative results.

II. THEORY OF THE ELECTROMAGNETIC MASS SHIFT

A. Introduction

It has been suggested[1] that when an electron interacts with a classical, plane polarized electromagnetic field, a finite mass renormalization occurs such that the electron's observable mass increases, becoming

$$m_* = \left[m_o^2 + \left(\frac{ea}{c^2}\right)^2 \right]^{\frac{1}{2}} \simeq m_o + \frac{1}{2}\frac{e^2a^2}{m_o c^4} \qquad \text{(II-1)}$$

where m_o is the electron rest mass in the absence of the field, e is the electron charge, c is the speed of light in vacuum and a is the (real) scalar amplitude of the vector potential describing the field. The relative mass shift is defined by

$$\frac{m_*-m_o}{m_o} \equiv \frac{\delta m}{m} \simeq \frac{1}{2}\frac{e^2a^2}{(m_o c^2)^2} \quad . \qquad \text{(II-2)}$$

In this chapter an argument is presented which is intended to show that the dominant effect of a plane wave field on a hydrogen-like atom is to cause an observable shift in the electron mass which is in agreement with Eq. (II-1). The discussion below is similar to the one outlined by Reiss[2] for the hydrogen atom, but it is more detailed because it does not neglect effects due to the electron spin. A non-relativistic wave equation is obtained, for hydrogen-like atoms, which displays the mass-shift effect explicitly up to and including the Zeeman energy and spin-orbit coupling terms. Perturbation theory is applied to the eigenfunctions of the approximate Hamiltonian, and the usual Fermi formula for the hfs splitting is obtained, and it also displays the mass

shift. Finally, an examination will be made of the dependence of the hyperfine-structure Zeeman levels on the electron mass.

B. Origin of the Mass Shift Hypothesis

As shown in Appendix A, the interaction of a spin 1/2 particle with external electric and magnetic fields can be described by the following equation:

$$(E-e\phi)^2\psi = [c^2(\vec{p} - \frac{e}{c}\vec{A})^2 + (mc^2)^2 - ec\hbar(\vec{\sigma}\cdot\vec{B} - i\vec{\alpha}\cdot\vec{E})]\psi \qquad \text{(II-3)}$$

where

$$\vec{B} = \nabla \times \vec{A}$$

and

$$\vec{E} = -\frac{1}{c}\frac{\partial\vec{A}}{\partial t} - \nabla\phi \quad .$$

The electric field $\vec{E}$ will always be written with an arrow so that it will not be confused with the total energy operator, $E = i\hbar\frac{\partial}{\partial t}$. The other quantities appearing in Eq. (II-3) have their usual meanings (see Appendix A).

Consider the following vector potential:

$$\vec{A} = \vec{A}_{rot} + \vec{A}_s \qquad \text{(II-4)}$$

where

$$\vec{A}_{rot} = a\,\mathrm{Re}[(\hat{y} \pm i\hat{z})\, e^{-i(\omega t - kx)}] \qquad \text{(II-5)}$$

is the vector potential of a circularly polarized plane wave of angular frequency $\omega = ck$ propagating in the +x direction with velocity c and amplitude a, and

$$\vec{A}_s = -B_o\, y\, \hat{x} \qquad \text{(II-6)}$$

is the vector potential of a uniform, static magnetic field, $\vec{B} = B_o \hat{z}$. The commonly used potential $\vec{A}_m = \frac{1}{2} \vec{B} \times \vec{r} = \frac{1}{2} B_o(x\hat{y}-y\hat{x})$ may be obtained from $\vec{A}_s$ by the gauge transformation $\vec{A}_m = \vec{A}_s + \nabla G$, where $G = \frac{1}{2} B_o xy$. Since Eq. (II-3) is invariant under gauge transformations, no generality is lost in the above choice for the form of $\vec{A}_s$. When Eq. (II-4) is inserted into Eq. (II-3), one obtains

$$(E-e\phi)^2\psi = \left[c^2(\vec{p} - \frac{e}{c}\vec{A}_s)^2 + (mc^2)^2 + e^2A_{rot}^2 - ec\hbar(\vec{\sigma}\cdot\vec{B}_s - i\vec{\alpha}\cdot\vec{E}_s) \right.$$
$$\left. - 2ec\,\vec{A}_{rot}\cdot\vec{p} - ec\hbar(\vec{\sigma}\cdot\vec{B}_{rot} - i\vec{\alpha}\cdot\vec{E}_{rot}) \right]\psi \quad , \qquad \text{(II-7)}$$

where the subscripts "rot" and "s" refer to the plane wave field and the static fields, respectively. In order to keep the wave equation time-independent, the last three terms in Eq. (II-7), which depend explicitly on time through $\vec{A}_{rot}$, $\vec{B}_{rot}$, and $\vec{E}_{rot}$ will be temporarily ignored. It will be shown in Sec. E of this chapter that for the frequencies of interest, the two terms involving $\vec{B}_{rot}$ and $\vec{E}_{rot}$ are of small magnitude compared to the $e^2A_{rot}^2$ term and compared to the terms containing $\vec{B}_s$ and $\vec{E}_s$ (Zeeman effect and spin-orbit coupling). These two terms can be satisfactorily accounted for through the use of time-dependent perturbation theory. The $\vec{A}_{rot}\cdot\vec{p}$ term, on the other hand, will be shown to be of the same order as the $e^2A_{rot}^2$ term; suggesting that, for the sake of consistency, one should drop the $e^2A_{rot}^2$ term at this point as well.

Once the last three time-dependent terms are dropped, the only term left in Eq. (II-7) involving the plane wave field is the $e^2A_{rot}^2$ term. From Eq. (II-5) one finds that

$$e^2 A_{rot}^2 = e^2 \vec{A}_{rot} \cdot \vec{A}_{rot} = e^2 a^2 \quad . \tag{II-8}$$

Since e^2a^2, like $(mc^2)^2$, is a constant scalar, it was suggested by Reiss that the e^2a^2 term serves as a finite mass renormalization, and that one should define an effective mass m_* by

$$(m_* c^2)^2 = (mc^2)^2 + e^2 a^2$$

which is the same as Eq. (II-1) above.

With the mass renormalization, Eq. (II-7) becomes, dropping the subscript "s" and ignoring the small time-dependent terms,

$$(E - e\phi)^2 \psi = \left[c^2 (\vec{p} - \frac{e\vec{A}}{c})^2 + (m_* c^2)^2 - ec\hbar(\vec{\sigma}\cdot\vec{B} - i\vec{\alpha}\cdot\vec{E}) \right] \psi \quad .$$

This equation is identical to the quadratic Dirac equation for a spin 1/2 particle of mass m_* in an external electromagnetic field.

Since all time-dependent terms have been dropped from Eq. (II-7), the time variation of ψ can be separated out and the operator E can be replaced by the total energy, also designated E. As a first step toward obtaining a non-relativistic wave equation, move the $(m_* c^2)^2$ term to the left-hand side and divide by $2m_* c^2$ to get

$$\left[\frac{E^2 - (m_* c^2)^2}{2m_* c^2} - \frac{Ee\phi}{m_* c^2} + \frac{e^2\phi^2}{2m_* c^2} \right] \psi = \left[\frac{1}{2m_*} (\vec{p} - \frac{e}{c}\vec{A})^2 - \frac{e\hbar}{2m_* c} (\vec{\sigma}\cdot\vec{B} - i\vec{\alpha}\cdot\vec{E}) \right] \psi \quad .$$

With the aid of the definition

$$W \equiv E - m_* c^2$$

the left-hand side can be rearranged to read

$$\text{LHS} = \frac{W^2 - 2e\phi W + e^2\phi^2}{2m_* c^2} + W - e\phi$$

$$= W - e\phi + \frac{1}{2m_* c^2}(W - e\phi)^2 \quad ,$$

so that the wave equation can be put into the form

$$\left[\frac{1}{2m_*}\left(\vec{p} - \frac{e}{c}\vec{A}\right)^2 + e\phi - \frac{e\hbar}{2m_* c}\left(\vec{\sigma}\cdot\vec{B} - i\vec{\alpha}\cdot\vec{E}\right) - \frac{1}{2m_* c^2}(W - e\phi)^2\right]\psi = W\psi \quad . \quad \text{(II-9)}$$

This equation is the same as the one given by Bethe and Salpeter[3] (their Eq. 12.9) for an electron in an external, static field, except that the electron mass has everywhere been replaced by m_*, the renormalized mass given by Eq. (II-1). [Bethe and Salpeter use a different convention than that employed here to represent the electron charge. As a result, Eq. (II-9) differs from their Eq. 12.9 by the sign of e.] In the next section this relativistic wave equation will be reduced to a non-relativistic approximation which contains terms only up to order $\frac{1}{m^2}$ or $(v/c)^2$ or $p^2/(mc)^2$. Since the last term in Eq. (II-9) is of the order $1/m^3$ it will be neglected. Hence the starting point for a reduction to a non-relativitic wave equation will be the following:

$$\left[\frac{1}{2m_*}\left(\vec{p} - \frac{e}{c}\vec{A}\right)^2 + e\phi - \frac{e\hbar}{2m_* c}\left(\vec{\sigma}\cdot\vec{B} - i\vec{\alpha}\cdot\vec{E}\right)\right]\psi = W\psi \quad . \quad \text{(II-10)}$$

C. The Non-Relativistic Wave Equation

Equation (II-10) is a relativistic equation describing a spin 1/2 particle of charge e and mass m_* in external, static electric and magnetic fields. The mass-shift effect should be observable for a

non-relativistic electron if the rotating field has sufficient intensity. Equation (II-10) can therefore be replaced by an approximate non-relativistic equation. In this section the relativistic Eq. (II-10) will be transformed, in the spirit of the Foldy-Wouthuysen method,[4] to obtain a non-relativistic Hamiltonian which contains Zeeman energy and spin-orbit coupling terms which are the same as in the usual non-relativistic theory[4] except that the electron mass is everywhere replaced by the renormalized mass m_* .

Let the four-component spinor wave function ψ be written as

$$\psi = \begin{pmatrix} \chi_1 \\ \chi_2 \end{pmatrix} \quad ,$$

where χ_1 and χ_2 are two-component spinors. If it were not for the $\vec{\alpha}\cdot\vec{E}$ term in Eq. (II-10), χ_1 and χ_2 would each obey the same differential equation. Because it contains the odd operator $\vec{\alpha}$, the $\vec{\alpha}\cdot\vec{E}$ term serves to couple χ_1 and χ_2. Equation (II-10) will now be transformed in such a way that terms involving $\vec{\alpha}$ which couple the positive and negative energy solutions χ_1 and χ_2 will be eliminated to order $(v/c)^2$, or equivalently, to order α^2 since α, the fine structure constant is equal to the ratio v/c for an electron in the (non-relativistic) hydrogen ground state. The result of the transformation will be an approximate wave equation for the two-component spinor χ_1 suitable for application to the hydrogen atom.

Begin by writing Eq. (II-10) in the form

$$H_0 \psi_0 = W\psi_0$$

$$H_0 = \frac{1}{2m_*}\vec{\pi}\cdot\vec{\pi} + e\phi - \frac{e\hbar}{2m_*c}\vec{\sigma}\cdot\vec{B} + \frac{ie\hbar}{2m_*c}\vec{\alpha}\cdot\vec{E} \quad . \tag{II-11}$$

Make the following unitary transformation

$$H_{nr} = e^{u} H_0 e^{-u}$$

$$\psi_{nr} = e^{u}\psi_0$$

where
$$u = \frac{\vec{\alpha}\cdot\vec{\pi}}{2m_*c} \quad . \tag{II-12}$$

The unitary of the transformation can be established by using the identity

$$e^{A}Be^{-A} = B + [A,B] + \frac{1}{2!}[A,[A,B]] + \frac{1}{3!}[A,[A,[A,B]]] + \cdots \tag{II-13}$$

The plan is to consider the transformation of H_0 term by term. Since u commutes with $\vec{\pi}$, it follows from the above identity that

$$e^{u}\frac{1}{2m_*}\vec{\pi}\cdot\vec{\pi}\,e^{-u} = \frac{1}{2m_*}\vec{\pi}\cdot\vec{\pi} \quad . \tag{II-14}$$

Consider the transformation of the second term:

$$e^{u}e\phi e^{-u} = e\phi + \frac{1}{2m_*c}[\vec{\alpha}\cdot\vec{\pi},e\phi] + \frac{1}{8m_*^2c^2}[\vec{\alpha}\cdot\vec{\pi},[\vec{\alpha}\cdot\vec{\pi},e\phi]] \quad .$$

It can be verified by a straightforward expansion that

$$[\vec{\alpha}\cdot\vec{\pi},e\phi] = -ie\hbar\vec{\alpha}\cdot\vec{E} \quad . \tag{II-15}$$

The application of the identity

$$(\vec{\sigma}\cdot\vec{A})(\vec{\sigma}\cdot\vec{B}) = \vec{A}\cdot\vec{B} + i\vec{\sigma}\cdot\vec{A}\times\vec{B} \tag{II-16}$$

leads to the result

$$[\vec{\alpha}\cdot\vec{\pi},\vec{\alpha}\cdot\vec{E}] = [\vec{\sigma}\cdot\vec{\pi},\vec{\sigma}\cdot\vec{E}] = -i\hbar\nabla\cdot\vec{E} + i\sigma\cdot(\vec{\pi}\times\vec{E} - \vec{E}\times\vec{\pi}) \quad . \tag{II-17}$$

With the aid of Eqs. (II-15) and (II-17), the transformation of the $e\phi$ term in H_0 becomes

$$e^{u}e\phi e^{-u} = e\phi - \frac{ie\hbar}{2m_*c}\vec{\alpha}\cdot\vec{E} + \frac{e\hbar}{8(m_*c)^2}\vec{\sigma}\cdot(\vec{\pi}\times\vec{E} - \vec{E}\times\vec{\pi}) - \frac{e}{8}\left(\frac{\hbar}{m_*c}\right)^2\nabla\cdot\vec{E} \quad . \tag{II-18}$$

With the use of Eq. (II-16) and the identity

$$\vec{\pi}\times\vec{\pi} = ie\vec{B} \tag{II-19}$$

it can be shown that the commutator $[\vec{\alpha}\cdot\vec{\pi},\vec{\sigma}\cdot\vec{B}]$ vanishes identically, and therefore that

$$e^{u}\left(-\frac{e\hbar}{2m_*c}\right)\vec{\sigma}\cdot\vec{B}\, e^{-u} = -\frac{e\hbar}{2m_*c}\vec{\sigma}\cdot\vec{B} \quad . \tag{II-20}$$

Finally, the transformation of the $\vec{\alpha}\cdot\vec{E}$ term in H_0 is

$$e^{u}\frac{ie\hbar}{2m_*c}\vec{\alpha}\cdot\vec{E}\, e^{-u} = \frac{ie\hbar}{2m_*c}\vec{\alpha}\cdot\vec{E} + \frac{ie\hbar}{4(m_*c)^2}[\vec{\alpha}\cdot\vec{\pi},\vec{\alpha}\cdot\vec{E}] \quad .$$

With the aid of Eq. (II-17), this becomes

$$e^{u}\frac{ie\hbar}{2m_*c}\vec{\alpha}\cdot\vec{E}\, e^{-u} = \frac{ie\hbar}{2m_*c}\vec{\alpha}\cdot\vec{E} - \frac{e\hbar}{4(m_*c)^2}\vec{\sigma}\cdot(\vec{\pi}\times\vec{E} - \vec{E}\times\vec{\pi}) + \frac{e}{4}\left(\frac{\hbar}{m_*c}\right)^2\nabla\cdot\vec{E} \quad . \tag{II-21}$$

When Eqs. (II-14), (II-18), (II-20), and (II-21) are combined, one obtains

$$H_{nr} = \frac{1}{2m_*}\left(\vec{p}-\frac{e}{c}\vec{A}\right)^2 + e\phi - \frac{e\hbar}{2m_*c}\vec{\sigma}\cdot\vec{B} - \frac{e\hbar}{2m_*c}\frac{\vec{\sigma}}{2}\cdot\frac{(\vec{\pi}\times\vec{E}-\vec{E}\times\vec{\pi})}{2m_*c} + \frac{e}{8}\left(\frac{\hbar}{m_*c}\right)^2\nabla\cdot\vec{E} \tag{II-22}$$

which is free of odd operators to order $(m_*c)^{-2}$. By a straightforward expansion, one can verify that

$$\vec{\pi}\times\vec{E} - \vec{E}\times\vec{\pi} = \vec{p}\times\vec{E} - 2(\vec{E}\times\vec{\pi}) \quad ,$$

so that Eq. (II-22) becomes

$$H_{nr} = \frac{1}{2m_*}\left(\vec{p} - \frac{e}{c}\vec{A}\right)^2 + e\phi - \frac{e\hbar}{2m_*c}\vec{\sigma}\cdot\vec{B} + \frac{e\hbar}{2m_*c}\frac{\vec{\sigma}}{2}\cdot\frac{\vec{E}\times\vec{\pi}}{m_*c} - \frac{1}{4}\frac{e\hbar}{2m_*c}\vec{\sigma}\cdot\frac{\vec{p}\times\vec{E}}{m_*c} + \frac{e}{8}\left(\frac{\hbar}{m_*c}\right)^2\nabla\cdot\vec{E} \quad . \tag{II-23}$$

Equation (II-23) is essentially the desired non-relativistic Hamiltonian. An interpretation of the various terms appearing in H_{nr} will be given before writing it in its final form. The first two terms make up the Hamiltonian in the Schrodinger theory of an electron of mass m_* in an electromagnetic field. If just these terms were taken as the approximate Hamiltonian, the resulting problem for a Coulomb potential and no magnetic field would be identical to the elementary hydrogen problem. It would yield the same energy level scheme (gross structure) as the non-relativistic problem but the electron mass would be changed from m to m_* in the Rydberg energy, i.e.,

$$Ry = \frac{1}{2}\alpha^2 mc^2 \rightarrow \frac{1}{2}\alpha^2 m_*c^2 \quad .$$

The third term in H_{nr} is the interaction energy of a magnetic dipole

$$\vec{\mu}_e = \frac{e\hbar}{2m_*c}\vec{\sigma} \tag{II-24}$$

with the external magnetic field $\vec{B}$. This is identical to the dipole moment obtained without the plane wave field except that the electron rest mass has now been replaced by the renormalized mass m_*

The last term in H_{nr}, the so-called Darwin term, gives a relativistic shift to s-states for a Coulomb field. It can be interpreted as an additional energy due to the electron's Zitterbewegung.

The next to last term is the interaction energy of the electron's magnetic dipole moment with a motional magnetic field, i.e.,

$$\frac{1}{4}\vec{\mu}_e \cdot \frac{\vec{p}\times\vec{E}}{m_* c} = \frac{1}{4}\vec{\mu}_e \cdot \frac{m_*\vec{v}}{m_* c} \times \vec{E}$$

$$= \frac{1}{4}\vec{\mu}_e \cdot \frac{\vec{v}}{c} \times \vec{E}$$

$$= \frac{1}{4}\vec{\mu}_e \cdot \vec{B}_{mot} \quad . \tag{II-25}$$

The remaining term in H_{nr} represents the spin-orbit coupling. Ignoring the $\vec{E} \times \vec{A}$ term,

$$\frac{e\hbar}{2m_* c}\frac{\vec{\sigma}}{2} \cdot \frac{\vec{E}\times\vec{\pi}}{m_* c} = \frac{1}{2}\frac{\hbar}{(m_* c)^2}\vec{S} \cdot e\vec{E}\times\vec{p} \quad ,$$

where the electron spin operator $\vec{S}$ is

$$\vec{S} = \frac{1}{2}\vec{\sigma} \quad .$$

For a central potential, one can write

$$e\vec{E} = -\nabla\phi = -\frac{1}{r}\frac{d\phi}{dr}\vec{r}$$

so that, with $\vec{L} = \vec{r} \times \vec{p}$,

$$\frac{e\hbar}{2m_* c}\frac{\vec{\sigma}}{2} \cdot \frac{\vec{E}\times\vec{\pi}}{m_* c} = -\frac{1}{2}\frac{\hbar}{(m_* c)^2}\frac{1}{r}\frac{d\phi}{dr}\vec{S}\cdot\vec{L} \quad . \tag{II-26}$$

Note that Eq. (II-26) contains the correct factor of 1/2 (Thomas factor). Equation (II-26) is in the usual form of the spin-orbit interaction energy but, once again, the electron mass has been replaced by the renormalized mass m_*.

The starting point is the non-relativistic Hamiltonian, Eq. (II-27). Neglecting terms that are quadratic in the vector potential $\vec{A}$, the interaction with the magnetic field is

$$\mathcal{H} = -\frac{e}{2m_*c} 2\vec{A}\cdot\vec{p} - \frac{e\hbar}{2m_*c} 2\vec{S}\cdot\vec{B}$$

or

$$\mathcal{H} = -2\mu_e\left(\frac{1}{\hbar}\vec{A}\cdot\vec{p} + \vec{S}\cdot\vec{B}\right)$$

where $S = \frac{1}{2}\vec{\sigma}$ is the electron spin angular momentum. A nucleus possessing a static magnetic dipole moment $\vec{\mu}$ produces a static magnetic field $\vec{B}$ derivable from the vector potential

$$\vec{A} = \frac{\vec{\mu}\times\vec{r}}{r^3} = -\vec{\mu}\times\left(\nabla\frac{1}{r}\right) \quad ,$$

i.e.,

$$\vec{B} = \nabla\times\vec{A} \quad .$$

The Hamiltonian for the magnetic dipole hyperfine interaction can therefore be written

$$\mathcal{H}_{hfs} = -2\mu_e\left\{\frac{1}{\hbar}\frac{\vec{\mu}\times\vec{r}}{r^3}\cdot\vec{p} - \vec{S}\cdot\nabla\times\left[\vec{\mu}\times\left(\nabla\frac{1}{r}\right)\right]\right\} \quad .$$

With the aid of standard vector identities, and by taking due care for the behavior at the origin, this can be written as

$$\mathcal{H}_{hfs} = -2\mu_e\left\{-\frac{1}{r^3}\vec{\mu}\cdot\vec{L} - \frac{8}{3}\pi(\vec{S}\cdot\vec{\mu})\delta(\vec{r}) - \frac{1}{r^3}\left[2(\vec{\mu}\cdot\hat{r})(\vec{S}\cdot\hat{r}) - \vec{\mu}\cdot\vec{S}\right]\right\} . \quad \text{(II-28)}$$

The correction to the ground state energy due to $\mathcal{H}_{hfs}$ is, to first order,

$$W_{hfs} = \langle 0|\mathcal{H}_{hfs}|0\rangle \quad .$$

In the ground state of a hydrogen-like atom $\vec{L} = 0$, so the first term in $\mathcal{H}_{hfs}$ gives no contribution. The last term is odd under inversion and therefore cannot have non-vanishing matrix elements between states of the same parity. One is left with

$$W_{hfs} = \langle 0 | \frac{16\pi}{3} \mu_e \, (\vec{S}\cdot\vec{\mu}) \, \delta(\vec{r}) | 0 \rangle$$

or

$$W_{hfs} = \frac{16\pi}{3} \mu_e \, |\psi_0(0)|^2 \, \langle \vec{S}\cdot\vec{\mu} \rangle \quad .$$

Since $\vec{S}$, $\vec{I}$, and $\vec{F} = \vec{S} + \vec{I}$ all commute with the Hamiltonian, S^2, F^2, and I^2 are good quantum numbers, and the expectation value of $\vec{S}\cdot\vec{\mu}$ can be evaluated for eigenstates of angular momentum.

Writing

$$\vec{\mu} = \frac{\mu}{I} \vec{I}$$

one obtains

$$\langle \vec{S}\cdot\vec{\mu} \rangle = \frac{\mu_I}{I} \langle \vec{S}\cdot\vec{I} \rangle \quad .$$

Squaring both sides of $\vec{F} = \vec{S} + \vec{I}$, and solving for the product $\vec{S}\cdot\vec{I}$, one obtains

$$\langle Fm_F | \vec{S}\cdot\vec{I} | Fm_F \rangle = \frac{1}{2} \langle Fm_F | \vec{F}\cdot\vec{F} - \vec{S}\cdot\vec{S} - \vec{I}\cdot\vec{I} | Fm_F \rangle$$

or

$$\langle \vec{S}\cdot\vec{I} \rangle = \frac{1}{2} [F(F+1) - S(S+1) - I(I+1)] \quad .$$

The energy of the hyperfine state now becomes

$$W_{hfs} = \frac{8\pi}{3} \mu_e \frac{\mu}{I} |\psi_0(0)|^2 \, [F(F+1) - S(S+1) - I(I+1)] \quad .$$

The energy difference between the two states F = I + S and F = I + S-1 is found to be

$$\Delta W = \frac{8\pi}{3} \mu_e \frac{\mu}{I} |\psi_0(0)|^2 \, 2F \quad .$$

With S = 1/2, 2F = 2(I+1/2) = 2I+1, and

$$\Delta W = \frac{8\pi}{3} \frac{2I+1}{I} \mu_e \mu_I |\psi_0(0)|^2 \qquad \text{(II-29)}$$

where the nuclear spin has been designated μ_I instead of simply μ.

Equation (II-29) is known as the Fermi formula, and ΔW, known as the zero-field hfs separation energy, is the energy separation between the two hfs levels of the $^2S_{1/2}$ ground state.

It remains to show how the Zeeman sublevels of the hfs are affected when the electron mass changes. A brief sketch will be given here of the derivation of the Breit-Rabi formula.[7] Two terms must be added to the hfs Hamiltonian [Eq. (II-28)] to describe the interaction of the electronic and nuclear magnetic dipole moments with an external, static magnetic field. The electronic contribution to the interaction is obtained from Eq. (II-27):

$$\mathcal{H}_{el} = - \frac{e}{m_* c} \vec{A} \cdot \vec{p} - \vec{\mu}_e \cdot \vec{B} \quad .$$

Equation (II-27) is based, in part, on the assumption that the nucleus is a point electric monopole, and therefore, as was done with $\mathcal{H}_{hfs}$, corrections for higher multipole nuclear moments must be added. The appropriate perturbation Hamiltonian is

$$\mathcal{H} = - \frac{e}{m_* c} \vec{A} \cdot \vec{p} - \vec{\mu}_e \cdot \vec{B} - \vec{\mu}_I \cdot \vec{B} + \mathcal{H}_{hfs} \quad .$$

Consider the first term. When $\vec{A} = -By\hat{x}$, then

$$-\frac{e}{m_* c}\vec{A}\cdot\vec{p} = \frac{eB}{m_* c} yp_x \quad .$$

This has the form of an electric quadrupole interaction whose matrix elements vanish in a $J = 1/2$ state.

Owing to the result for $\mathcal{H}_{hfs}$, it is possible to write

$$\mathcal{H}_{hfs} = h\alpha\, \vec{I}\cdot\vec{S}$$

where α (not to be confused with the plane wave field amplitude a) can be calculated fairly accurately for hydrogen with the Fermi formula but has been determined experimentally to a very high precision for hydrogen[8] and for the other stable alkalis.[9,10,11,12,13] The total hyperfine interaction can therefore be written

$$\mathcal{H} = h\alpha\, \vec{I}\cdot\vec{S} - \vec{\mu}_I\cdot\vec{B} - \vec{\mu}_e\cdot\vec{B} \quad .$$

The eigenvalue problem to be solved is

$$\mathcal{H}\psi = E\psi$$

where ψ is an eigenstate of the total angular momentum $\vec{F}$. The secular equation $(\mathcal{H}-EI)\psi = 0$ must be solved for the eigenvalues E. Since F_z commutes with $\mathcal{H}$, $\mathcal{H}$ can only connect states which have the same m_F , i.e., $\langle F'm_F'|\mathcal{H}|Fm_F\rangle = 0$ if $m_F' \neq m_F$.

The application of standard, degenerate perturbation theory[14] leads to the Breit-Rabi formula for the energy of the state $|F\ m_F\rangle$ as a function of applied field:

$$E = -\frac{\Delta W}{2(2I+1)} - \frac{\mu_I}{I} H_0 m_F \pm \frac{\Delta W}{2}\left(1 + \frac{4m_F}{2I+1} x + x^2\right)^{1/2} \qquad \text{(II-30)}$$

where

$$x \equiv (\mu_I/I - \mu_e/S)\, H_0/\Delta W$$

and

$$\Delta W = \frac{1}{2} h\alpha(2I+1) \quad .$$

The minus sign in this equation is used for the states $F = I-1/2$, $m_F = F, F-1, \cdots, -F$, while the plus sign is used for the states $F = I+1/2$, $m_F = F, F-1, \cdots, -(F-1)$. The energy of the state $|I+1/2, -(I+1/2)\rangle$ is found by using the plus sign when $x < 1$ and the minus sign when $x > 1$.

The change in the hfs energy levels due to a change in the electron mass can be obtained by differentiating the Breit-Rabi formula with respect to the electron mass. The hydrogen wave function can be used to evaluate $|\psi_0(0)|^2$ in the Fermi formula so that the explicit mass dependence of ΔW can be ascertained. Using $|\psi_0(0)|^2 = \frac{1}{\pi}(Ze^2)^3 m_*^2/\hbar^6$ and $\mu_e = \frac{e\hbar}{2mc}$, one finds

$$\Delta W \propto m^2$$

and

$$\delta(\Delta W) = 2\frac{\delta m}{m}\Delta W \ , \qquad \text{(II-31)}$$

where $\frac{\delta m}{m}$ is the electron's relative mass shift. In the same fashion one can write

$$x = \frac{\mu_I}{I}\frac{H_0}{\Delta W} - \frac{\mu_e}{S}\frac{H_0}{\Delta W} \propto c_1 m^{-2} + c_2 m^{-3}$$

where c_1 and c_2 do not depend upon m. The change in x due to a change in m is

$$\delta x = \frac{\delta m}{m} \frac{H_0}{\Delta W} \left(- \frac{2\mu_I}{I} + \frac{3\mu_e}{S} \right) \quad .$$

With these results for $\delta(\Delta W)$ and δx, one obtains, after a straightforward differentiation of the Breit-Rabi formula,

$$\delta W = \frac{\delta m}{m} \left[- \frac{\Delta W}{2I+1} \pm \Delta W R \pm \frac{H_0}{2R} \left(- \frac{2\mu_I}{I} + \frac{3\mu_e}{S} \right) \left(\frac{2m_F}{2I+1} + x \right) \right] \qquad \text{(II-32)}$$

where

$$R = \left(1 + \frac{4m_F}{2I+1} x + x^2 \right)^{\frac{1}{2}} \quad .$$

Equation (II-32) gives the change in energy of the hfs level $|F\ m_F\rangle$ due to a relative change $\frac{\delta m}{m}$ in the mass of the electron. This shift is not the same for all hyperfine levels as indicated by the dependence of δW on m_F and F (i.e., through the ± sign). The frequency shift for a transition between levels of energy W_1 and W_2 due to a shift in the electron mass is given by

$$\delta \nu = \frac{\delta W_1 - \delta W_2}{h} \propto \frac{\delta m}{m} \quad . \qquad \text{(II-33)}$$

It turns out that the proportionality constant in Eq. (II-33) is of order unity for most cases of experimental interest. Hence the shift of a transition frequency is proportional to the relative mass shift, and a relative mass shift of, say, 10^{-6} results in a transition frequency shift of the same magnitude.

E. Consideration of Small, Time-Dependent Terms

In the previous sections the following three terms were neglected:

$$\mathcal{H}_{rot} = -\frac{e}{m_* c}\vec{A}_{rot}\cdot\vec{p} - \frac{e\hbar}{2m_* c}(\vec{\sigma}\cdot\vec{B}_{rot} - i\vec{\alpha}\cdot\vec{E}_{rot}) \quad . \tag{II-34}$$

They were neglected in order that a time-independent Hamiltonian could be obtained whose eigenfunctions would be stationary states. In order to get an estimate of their importance they will be treated as time-dependent perturbations of the stationary ground state which is an eigenfunction of the time-independent Hamiltonian Eq. (II-27). It will be assumed that the only static vector potential is that due to the hyperfine interaction (see Sec. D above), in the absence of external magnetic fields. Any time-dependent perturbation can be broken up into its Fourier components, each of which can be studied separately. A typical component may be written in the form

$$\mathcal{H}b = Ve^{-i\omega t}, \quad V \neq V(t) \quad . \tag{II-35}$$

The resulting transition probabilities, mixing parameters and energy level shifts, are proportional to the matrix elements of V between stationary states. The following discussion can therefore be simplified by dropping the factor $e^{-i\omega t}$ from $\vec{A}_{rot}$, $\vec{B}_{rot}$, and $\vec{E}_{rot}$.

The last two terms in Eq. (II-34) can be expressed in the form of a magnetic dipole interaction. For a circularly polarized plane wave $\vec{E} = \pm i\vec{B}$ so that these terms can be written, dropping the subscript "rot",

$$\frac{e\hbar}{2m_* c}(\vec{\sigma}\cdot\vec{B} - i\vec{\alpha}\cdot\vec{E}) = \frac{e\hbar}{2m_* c}(\vec{\sigma}\cdot\vec{B} \pm \vec{\alpha}\cdot\vec{B}) = \vec{\mu}_e\cdot\vec{B}\begin{pmatrix} I & \pm I \\ \pm I & I \end{pmatrix} \quad .$$

This term has the form of a Zeeman energy. Since perturbation theory will be used on the ground state hfs, this term should be kept smaller than the hfs separation energy. For example, $E_{hfs} = 6.6 \times 10^{-6}$ eV, for an hfs separation frequency of 10 GHz, while $\vec{\mu}_e \cdot \vec{B} = 5.8 \times 10^{-9}$ eV when B is one gauss.

This Zeeman energy term can be written in the form

$$\mathcal{H}_{rf} = \vec{\mu}_e \cdot \vec{H}_{rf} \, e^{-i\omega t} \quad .$$

The treatment of such a term by time-dependent perturbation theory yields transition probabilities[15] for magnetic dipole transitions when ω is near a transition frequency and small frequency shifts[16] (Bloch-Siegert effect) when it is not. These frequency shifts will be discussed in more detail in Chapter IV where it will be shown that they are three orders of magnitude smaller than expected frequency shifts due to the electron mass shift.

It should be pointed out under what conditions this term is small compared to the e^2a^2 mass renormalization term. The comparison is to be made between $e\hbar c\vec{\sigma}\cdot\vec{B}$ and e^2a^2 since this is the way the two terms appeared in Eq. (II-7), prior to the dropping of the time-dependent terms. For low magnetic fields $|\vec{\sigma}\cdot\vec{B}| = m_F \, |B| = m_F \frac{\omega}{c} a$ since $\vec{B} = \nabla \times \vec{A} = \pm \frac{\omega}{c} \vec{A}$. Thus,

$$\frac{e\hbar c\vec{\sigma}\cdot\vec{B}}{e^2a^2} = \frac{e\hbar c \, m_F \, \omega/c \, a}{e^2a^2} \sim \frac{\hbar\omega}{ea} \quad .$$

This Zeeman energy term will be much smaller than the mass renormalization term as long as

$$ea >> \hbar\omega \quad . \tag{II-36}$$

For $\omega/2\pi$ = 10 GHz, this requirement amounts to $ea >> 6.6 \times 10^{-6}$ eV.

Consider the matrix element $\langle n'|\frac{e}{m_* c}\vec{A}_{rot}\cdot\vec{p}|n\rangle$ where $|n\rangle$ stands for $|njIFm_F\rangle$ which is an hfs sublevel of the $|nj\rangle$ eigenstate. In first-order perturbation theory, only the ground state hfs sublevels need be considered, and the basis can be designated by $|Fm_F\rangle$. When $\hat{\varepsilon} = \hat{y} \pm i\hat{z}$ and $\vec{k} = k\hat{x}$, the vector potential can be written

$$\vec{A}_{rot} = aRe(\hat{\varepsilon}e^{i\vec{k}\cdot\vec{r}}) = a(\hat{y}\mp\hat{z}kx+\cdots) \ ,$$

and a typical matrix element takes the form

$$\langle n'|\frac{e}{m_* c}\vec{A}\cdot\vec{p}|n\rangle \simeq \frac{ea}{m_* c}\{\langle n'|p_y|n\rangle \mp k\langle n'|xp_z|n\rangle\} \quad . \tag{II-37}$$

The following four identities[3] hold whenever $H = p^2/2m_* + V$ and $[\vec{r},V] = 0$:

$$\vec{p} = -\frac{im_*}{\hbar}[\vec{r},H] \tag{II-38}$$

$$\langle m|\vec{p}|n\rangle = im_*\omega_{mn}\langle m|\vec{r}|n\rangle \tag{II-39}$$

$$\left.\begin{aligned} r_i p_j &= -\frac{1}{2}\frac{im_*}{\hbar}[r_i r_j,H] + \frac{1}{2}L_k \quad (i\neq j) \\ r_i p_i &= -\frac{1}{2}\frac{im_*}{\hbar}[r_i^2,H] + \frac{1}{2}i\hbar \end{aligned}\right\} \tag{II-40}$$

$$\left.\begin{aligned} \langle m|r_i p_j|n\rangle &= \frac{1}{2}im_*\omega_{mn}\langle m|r_i r_j|n\rangle + \frac{1}{2}\langle m|L_k|n\rangle \\ \langle m|r_i p_i|n\rangle &= \frac{1}{2}im_*\omega_{mn}\langle m|r_i^2|n\rangle + \frac{1}{2}i\hbar\delta_{mn} \end{aligned}\right\} \tag{II-41}$$

where

$$\omega_{mn} = (E_m - E_n)/\hbar$$

and $|m\rangle$ and $|n\rangle$ are eigenstates of H. Equations (II-39), (II-40), and (II-41) are corollaries of Eq. (II-38).

With the aid of Eq. (II-39) the first term in Eq. (II-37) becomes a matrix element of the position operator between two hfs levels. Such a matrix element must vanish since the ground state hfs levels all have the same parity. An application of Eq. (II-41) converts the second term into the matrix element of xz. ($\vec{L} = 0$ in the ground state so the expectation values of all of its components vanish.) This is essentially an electric quadrupole matrix element which vanishes because there can be no electric quadrupole interaction within a J = 1/2 state.

The second order correction to the ground state energy due to the interaction $-\frac{ea}{m_* c}\hat{y}\cdot\vec{p}$ is

$$E_0^{(2)} = \left(\frac{ea}{m_* c}\right)^2 \sum_{n\neq 0} \frac{\langle 0|p_y|n\rangle\langle n|p_y|0\rangle}{E_0^{(0)} - E_n^{(0)}}$$

where $|0\rangle$ represents any of the ground state hfs levels whose unperturbed energy is $E_0^{(0)}$, and $|n\rangle$ represents any hfs level of any other state. By the use of Eq. (II-39) this energy correction may be written as

$$E_0^{(2)} = \frac{e^2a^2}{m_* c^2}\frac{i}{\hbar}\sum_{n\neq 0}\langle 0|p_y|n\rangle\langle n|y|0\rangle$$

which becomes, upon application of closure

$$E_0^{(2)} = \frac{ie^2a^2}{\hbar m_* c^2}\{\langle 0|p_y y|0\rangle - \langle 0|p_y|0\rangle\langle 0|y|0\rangle\} \quad .$$

The second term in brackets vanishes as a result of the parity selection rule. With the aid of Eq. (II-41) the first term in the

brackets is just 1/2 ih. Hence

$$E_0^{(2)} = -\frac{e^2a^2}{2m_*c^2} \quad . \tag{II-42}$$

Now, if the e^2A^2 term in Eq. (II-7) were retained, instead of being used to renormalize the mass, it would persist through the transformations of Sections B and C above and appear in the resulting non-relativistic Hamiltonian as $e^2a^2/2mc^2$. Also, when the mass renormalization is not made, Eq. (II-42) reads $-e^2a^2/2mc^2$. Hence, the $\vec{A}\cdot\vec{p}$ term, taken to second order, exactly cancels the e^2A^2 term, taken to first order. These arguments based upon perturbation theory do not necessarily invalidate the mass-shift hypothesis. When, for example, the relative mass shift has the experimentally realizable value $\frac{\delta m}{m} = 2 \times 10^{-6}$, then

$$\frac{e^2a^2}{2mc^2} = \frac{e^2a^2}{2(mc^2)^2}\, mc^2 = \frac{\delta m}{m}\, mc^2 = 1 \text{ eV}$$

which is certainly not small compared even to the gross structure. It is therefore not clear that perturbation theory is the proper method for handling these terms.

F. Summary

It has been shown that when time-dependent terms are neglected, the principal effect of a circularly polarized plane wave field which interacts with a hydrogen-like atom is to cause a finite renormalization of the electron mass. This renormalization has been exhibited explicitly in the spin-orbit, hyperfine and Zeeman interactions as well as in the

gross structure. The effect of an electron mass increase on the hyperfine structure has been discussed, and it has been found that, if a mass change occurs, then frequency shifts should be the same order of magnitude as the relative mass shift. It has been pointed out that, if the mass renormalization is not made, then the effect of the time-dependent terms is to exactly cancel the mass renormalization term.

III. DESCRIPTION OF THE EXPERIMENT

A. Introduction

The atomic-beam magnetic-resonance technique was used in this search for an electron mass-shift effect in ^{133}Cs. The relatively high cesium transition frequencies ($\sim 10^{10}$Hz) together with the narrow linewidths ($\sim 10^{3}$ Hz) obtainable with the Ramsey separated-oscillatory-field method allow transition frequencies to be determined to a precision of a few parts in 10^{8}. Oscillating microwave fields of sufficient intensity to produce a relative mass shift of one part per million were produced in a resonant cavity powered by an inexpensive, mechanically-tuned magnetron.

B. Experimental System – ^{133}Cs Ground State hfs

1. Justification for Studying Cesium Rather Than Hydrogen: Although the theory of the electron mass shift was developed in Chapter II with the hydrogen atom in mind, it should apply to alkali atoms as long as the central field approximation is valid, i.e., as long as the valence electron experiences an electrostatic potential which is a function of radial position only. The non-central magnetic dipole interaction has already been accounted for by perturbation theory and has led to the hyperfine interaction described by the Fermi formula. The spherical symmetry of the $^{2}S_{1/2}$ electronic state forbids the existence of any multipole interactions beyond electric monopole and magnetic dipole.

Breit[1] and Kopfermann[2] have summarized some of the correction factors which should be applied to the Fermi formula before it is

used to deduce alkali nuclear magnetic dipole moments from measured hyperfine energy separations. Kopfermann gives the following expression for the hfs frequency:

$$\Delta\nu = \frac{8}{3}(2I+1)\frac{\mu_e}{h}\frac{\mu_I}{I}\frac{Z_i Z_a^3}{a_0^3 n_a^3}\left(1-\frac{d\sigma}{dn}\right)F_r(j,Z_i)(1-\delta)(1-\varepsilon) \quad . \qquad \text{(III-1)}$$

The factor $Z_i Z_a^2/n_a^3$ is a correction to $|\psi_0(0)|^2$ [see Eq. (II-29)] obtained by assuming that the valence electron is under the action of an effective nuclear charge eZ_a when it is outside the electron core, and that it is under the action of an effective nuclear charge eZ_i when its orbit is inside the electron core. For cesium[2] $Z_i = Z = 55$, $Z_a = 1$, and $n_a^3 = 6.53$. The factors $(1-\frac{d\sigma}{dn})$ and $F_r(j,Z_i)$ are relativistic corrections which do not involve the electron mass. The parameters δ and ε, which do depend upon the electron mass, correct for the fact that the nuclear charge and magnetic moments are distributed throughout (or on the surface of) a sphere of finite volume.

When these correction factors are taken into consideration, one obtains

$$\delta(\Delta\nu) = 1.96\,\frac{\delta m}{m}\,\Delta\nu \qquad \text{(III-2)}$$

which differs by only 2% from the result obtained above [Eq. (II-31)] assuming hydrogenic wave functions and no corrections to the Fermi formula.

Further corrections to the Fermi formula exist.[3] A reduced mass correction due to the finite nuclear mass contributes a factor of $(1 + M/m)^{-3}$ to Eq. (III-1) and a correction to Eq. (III-2) that

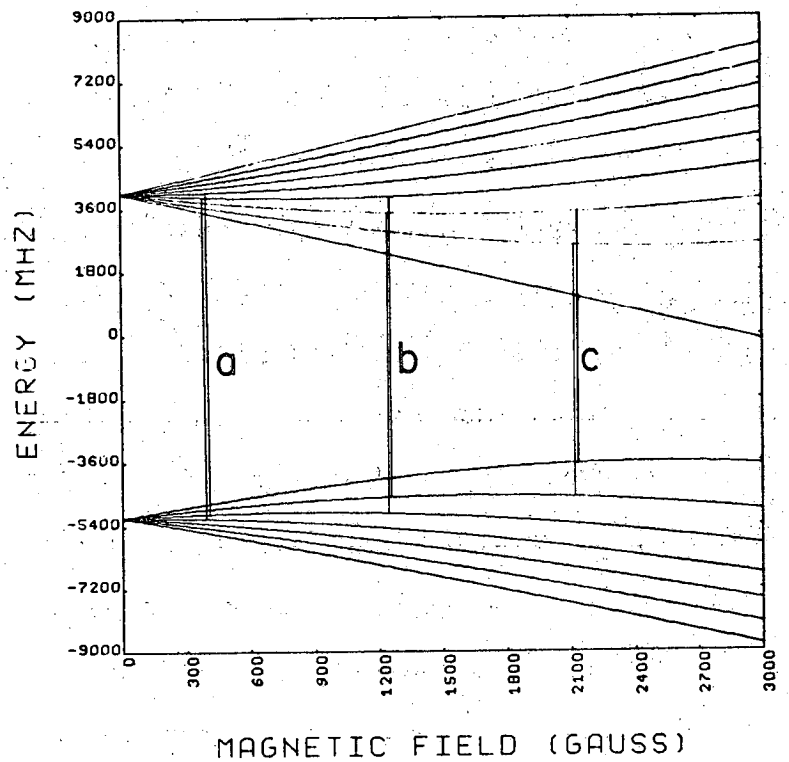

CURVES ARE ENUMERATED IN A CLOCKWISE ORDER ALONG THREE EDGES, STARTING IN THE UPPER LEFTHAND CORNER.

	F	m
1.	4.0	4.0
2.	4.0	3.0
3.	4.0	2.0
4.	4.0	1.0
5.	4.0	0.
6.	4.0	-1.0
7.	4.0	-2.0
8.	4.0	-3.0
9.	4.0	-4.0
10.	3.0	-3.0
11.	3.0	-2.0
12.	3.0	-1.0
13.	3.0	0.
14.	3.0	1.0
15.	3.0	2.0
16.	3.0	3.0

ATOM CS133 , STATE 6SJ1/2,
I = 3.5
A = 2298.157940MHZ
B = -0. MHZ
C = -0. MHZ
GJ= -2.002542
GI= 3.9899E-04

XBL 698-1147

Fig. III-1. ^{133}Cs ground state hyperfine-structure showing removal of degeneracy by static magnetic field.

magnetic dipole radiation are

$$\Delta F = 0, \pm 1$$

$$\Delta m_F = 0, \pm 1 \quad .$$

Transitions can be observed with the atomic-beam magnetic-resonance technique only if the initial and final states have opposite effective magnetic moments, defined by

$$\mu_{eff} = - \frac{\partial W}{\partial H}$$

where W is the energy of the state and H is the external field. Since μ_{eff} is just the slope of the W vs. H curve, one can see from Fig. III-1 that, for large fields, a change in the sign of the effective moment corresponds to a change in the sign of m_J. Therefore, when large deflecting (A and B) fields are used, the machine selection rule

$$\Delta m_J = \pm 1$$

does not permit observation of $\Delta F = 0$ transitions except for the so-called standard transition $|I + 1/2, -I + 1/2\rangle \leftrightarrow |I + 1/2, -I - 1/2\rangle$.

b. Field-Independent Transitions: Stimulated transitions will occur when an atom passes through a region where it is subjected to a time-varying field of the appropriate frequency and orientation. Since the lifetime for spontaneous transitions is so long compared to the transit time Δt of an atom traversing this interaction region, the linewidth (in Hz) can be found, from the uncertainty principle, to be

$$\Delta \nu \geq \frac{1}{\Delta t} \quad .$$

This linewidth can, in principle, be made as small as the natural linewidth for spontaneous transitions by increasing the transit time Δt, or, equivalently, by increasing the length of the interaction region.

Transitions usually take place inside laboratory magnetic fields, and it is not possible to produce perfectly uniform magnetic fields over arbitrarily long distances. Since transition frequencies, in general, depend upon the value of the external field H_0, any inhomogeneities in H_0 will cause transitions to occur at slightly different frequencies at different points along the interaction region. The net result is a broadening of the resonant line. Field inhomogeneities can be minimized by working at fields where the transition frequencies are only weakly dependent upon H_0. At those magnetic fields where $\frac{df}{dH} = 0$ the transition frequency f is independent, to first order, of magnetic field H. Such field values are referred to as field-independent points.

Table III-1 is a list of the field-independent $\Delta F = \pm 1$ transitions for ^{133}Cs. Four are of the σ type ($\Delta m_F = 0$) while six are of the π type ($\Delta m_F = \pm 1$). The six π transitions occur in three doublets which are labeled a, b and c in Fig. III-1. These three doublets were chosen for extensive study in the search for an electron mass shift.

C. Apparatus

A standard flop-in atomic-beam magnetic-resonance apparatus[3] utilizing the Ramsey separated-oscillatory-field technique[3] was used to investigate shifts of hfs transition frequencies that occurred as a cesium beam traversed a microwave cavity.

Table III-1. ^{133}Cs Field-Independent Transitions.

Designation	Field (Gauss)	Transition (F,m_F)	Type	Frequency (MHz)
	0	(4,0) ↔ (3,0)	σ	9192.631770
a_1	416	(4,-1) ↔ (3,0)	π	9119.6
a_2	417	(4,0) ↔ (3,-1)	π	9119.1
	820	(4,-1) ↔ (3,-1)	σ	8900.7
b_1	1252	(4,-2) ↔ (3,-1)	π	8509.5
b_2	1253	(4,-1) ↔ (3,-2)	π	8508.1
	1640	(4,-2) ↔ (3,-2)	σ	7961.0
c_1	2104	(4,-3) ↔ (3,-1)	π	7115.3
c_2	2105	(4,-2) ↔ (3,-3)	π	7112.9
	2460	(4,-3) ↔ (3,-3)	σ	6080.4

1. Beam Machine: Figure III-2 is a schematic representation of the atomic beam apparatus used for this experiment.

Cesium atoms are produced in a resistance heated steel oven by the reaction of calcium metal with a cesium halide, e.g.

$$Ca + 2CsC\ell + \text{heat} \rightarrow CaC\ell_2 + 2Cs \quad .$$

The oven shown in Fig. III-3 was designed to hold about 1-3/4 cm^3 of $CsC\ell$ and Ca filings mixed in the ratio of two parts (vol) Ca to one part $CsC\ell$. Such a charge is sufficient for about fifteen hours of running (4 runs). A full beam of about 6×10^{10} atoms/sec reaches the detector (detector current 10^{-9} A) when 60 W (2 A at 30 V) of ac power is dissipated in the filament. The filament is made from about eighteen inches of .010-in. thoriated tungsten or tantalum wire tightly wound on a .060-in. rod.

Atoms effuse from the oven through a .005-in. slit into the oven chamber where the pressure is typically 4×10^{-6} mm Hg. The beam then passes through a buffer chamber (7×10^{-7} mm Hg) and into the field of the A magnet. Typical pressures in the rest of the machine (A and B magnets, C magnet region and detector chamber) are all less than 3×10^{-7} mm Hg.

For the two angles of exit from the atomic beam oven in Fig. III-2 beam atoms in states of opposite m_J are deflected along different paths toward the machine axis by the inhomogeneous field of the A magnet ($H \sim 5$ kG, $\partial H/\partial Z \sim 5$ kG/cm). In the uniform field of the C magnet the beam is subjected to an appropriate microwave frequency of sufficient strength to cause a transition between two states of different

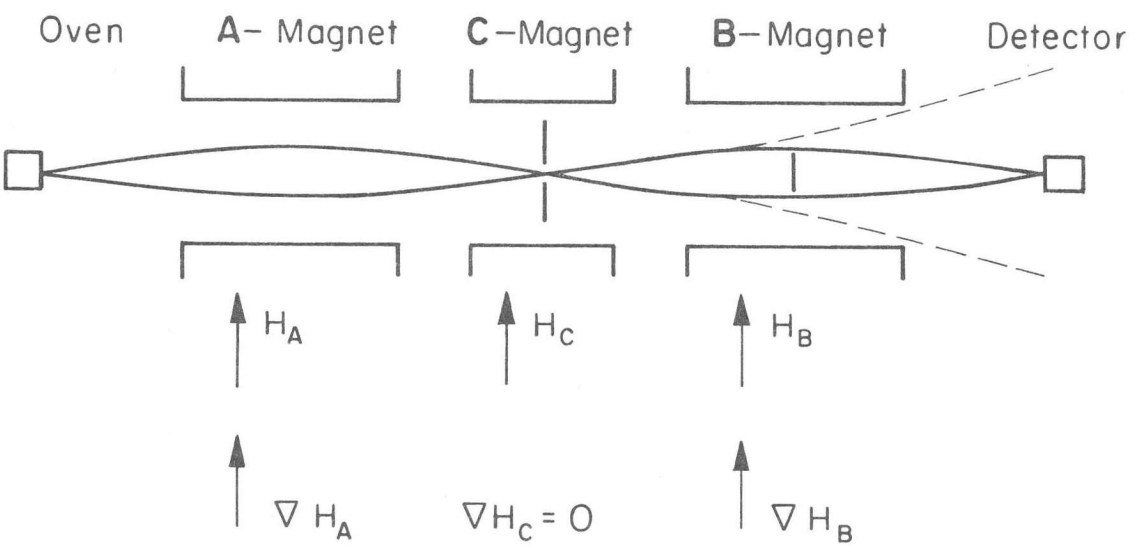

Fig. III-2. Flop-in type atomic-beam magnetic-resonance apparatus.

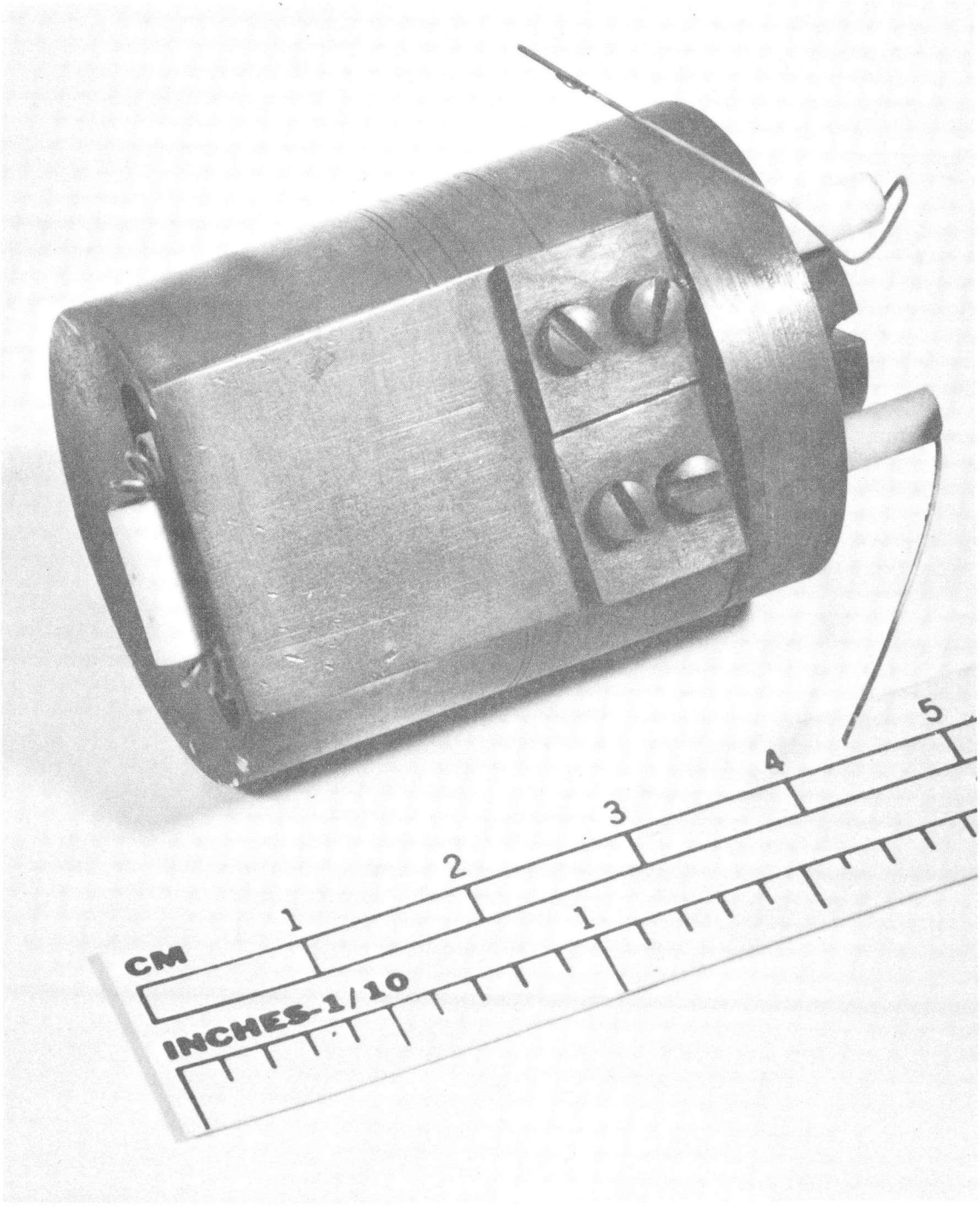

XBB 694-2182

Fig. III-3. Photograph of oven.

m_J. The sign of μ_{eff} is therefore reversed for atoms which undergo transitions, and the atoms are again deflected toward the machine axis (solid line in Fig. III-2) as they pass through the inhomogeneous B magnet where the field and gradient are the same as those in the A magnet. In this manner atoms which undergo transitions in the C region are said to be "focused" at the detector. Atoms which do not undergo transitions follow the dashed line in the B magnet and are not detected.

The detector is a standard tungsten hot wire ionization detector.[3] An atom whose ionization potential (3.87 V for Cs) is less than the work function of tungsten (4.5 V) will be ionized on impact and may be accelerated to a collector. The beam reaching the detector is hence converted into a current that is measured by a sensitive electrometer (Keithly model #417). The electrometer is capable of suppressing constant background currents up to 10^{-4} A, so that below that level the current is proportional to the beam intensity. For the flop-in arrangement used here, maximum current is registered at the detector when the frequency of the rf field in the transition region equals a transition frequency of the system under study.

2. Cavity-Hairpin Assembly: The actual experiment is performed in the C region (Fig. III-2) where appropriate resonant and non-resonant oscillating fields are introduced through the cavity-hairpin assembly. Two assemblies were built which could each be used with either of two cavities.

Figure III-4 is a photograph of one assembly with the cover removed to show the inside of the cavity. The beam passes from left

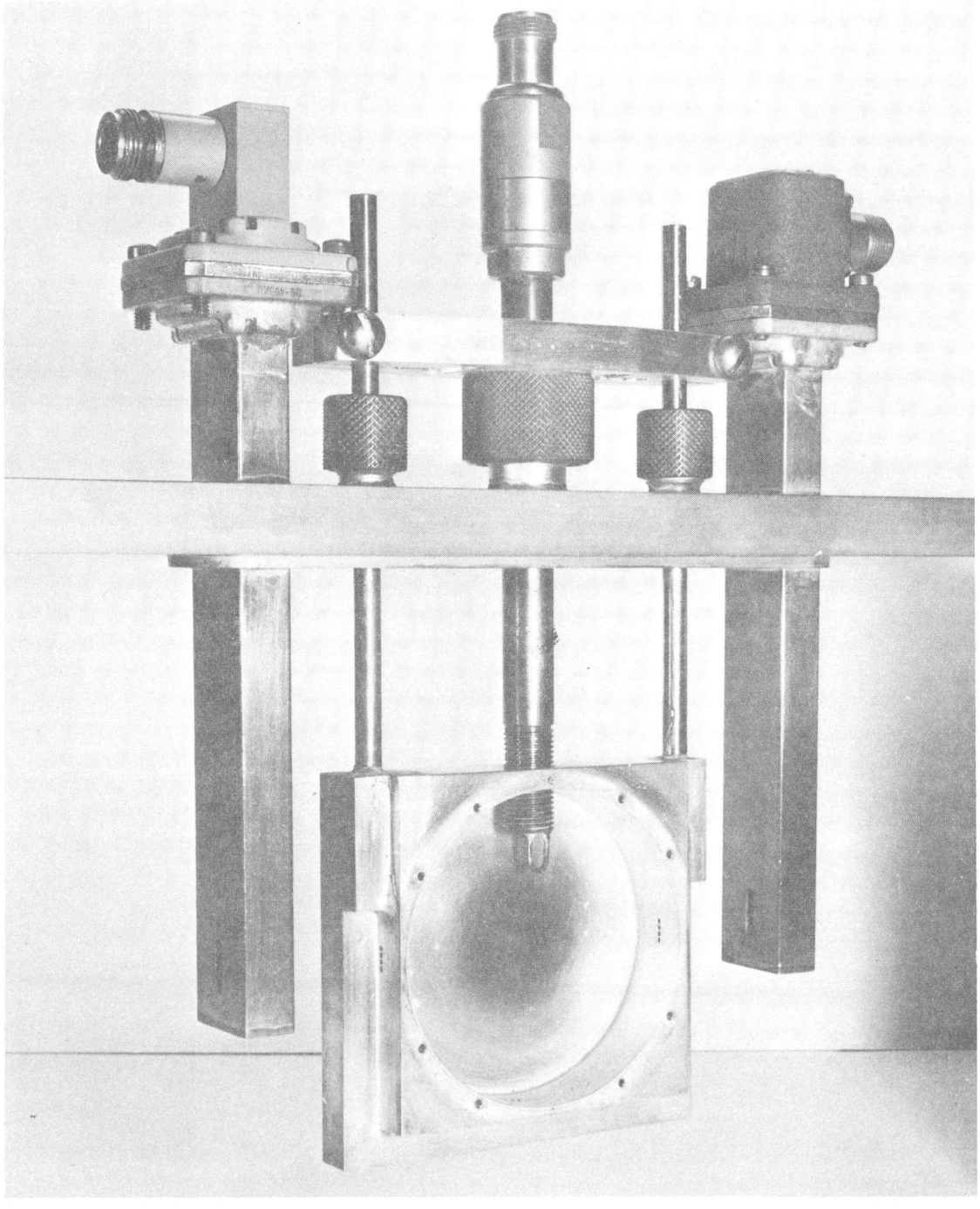

XBB 694-2179

Fig. III-4. Photograph of cavity-hairpin assembly showing interior of 2921 MHz TM_{010} cavity and coupling loop.

to right, and the static field H_0 is at right angles to the cavity faces. The entrance and exit apertures in the cavity each consist of four .055-in. diameter holes which serve to collimate the beam. The cavity shown was resonant at 2.921 GHz (TM_{010} mode). The two hairpins are made from shorted X-band (8.2 GHz to 12.4 GHz) waveguide. The rf magnetic field inside the waveguide is mostly parallel to H_0 and is appropriate for stimulating σ transitions (see Table III-1). The two smaller diameter tubes shown in the figure allow cooling water to circulate through the body of the cavity. Figure III-5 is a second photograph of this same assembly. Figure III-6 is a photograph showing the second assembly with a cavity designed to operate at 7.93 GHz (TM_{210} mode). These hairpins consist of loaded, 5/8-in., 50 Ω rigid coaxial transmission lines. These hairpins were used for virtually all the work reported here since they produce an oscillating magnetic field which is, for the most part, at right angles to H_0 and is appropriate for stimulating π transitions.

A high-powered, continuous wave microwave signal produced by a mechanically-tuned magnetron is fed into the constant field region via a 1/2-in., 50 Ω rigid coaxial transmission line and is inductively coupled to the cylindrical cavity. The coupler designed for this purpose is exposed in Fig. III-4. A loop of #20 copper wire is soldered to one end to form a coupling loop, and a type N coaxial connector (Times Wire & Cable #AMS-5012NF-18S) is attached to the other end. The end nearest the loop is threaded so the loop can be positioned

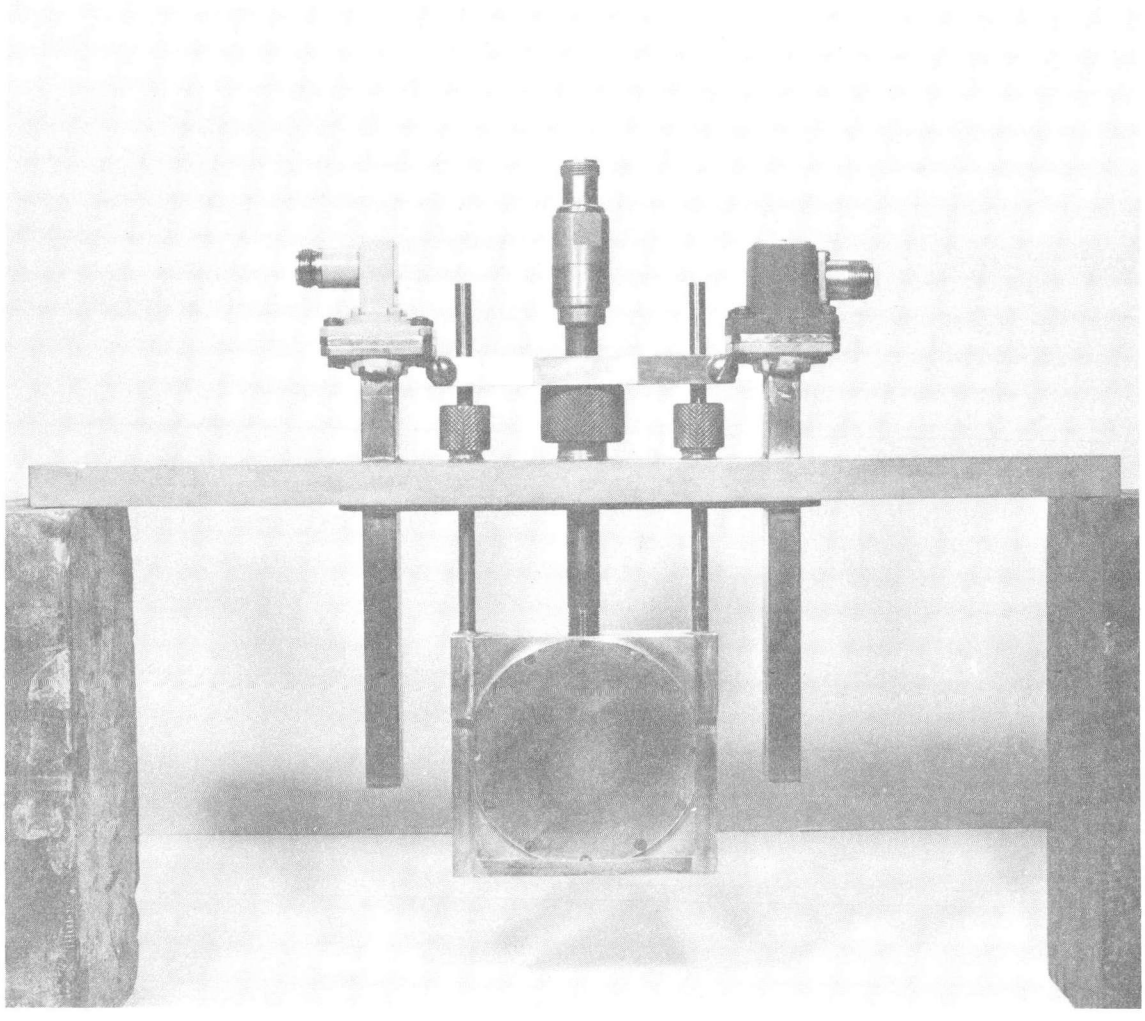

XBB 694-2181

Fig. III-5. Photograph of cavity-hairpin assembly. The waveguide hairpins shown here are suitable for studying $\Delta m_F = 0$ transitions in the frequency range 8.2 GHz to 12.4 GHz.

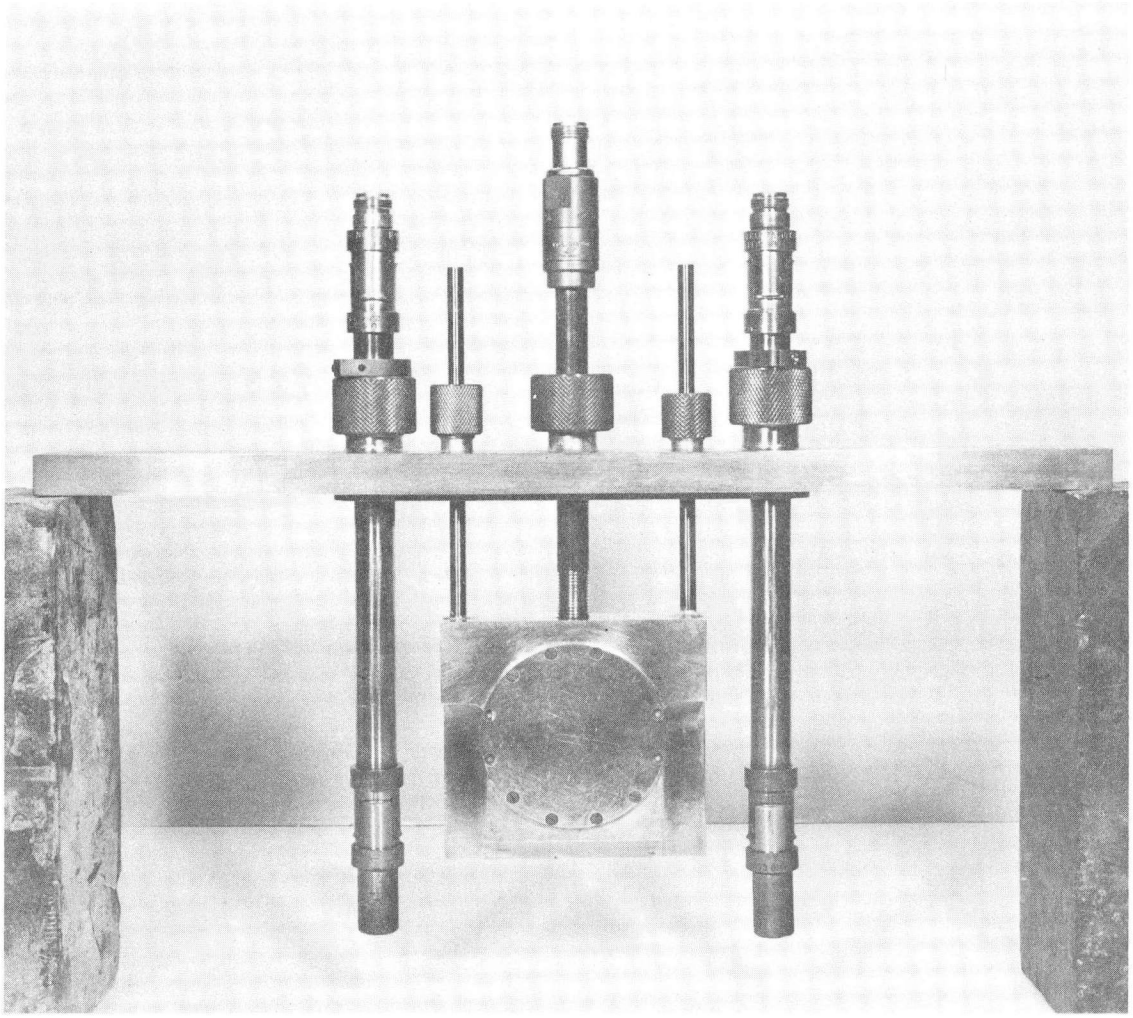

XBB 694-2180

Fig. III-6. Photograph of cavity-hairpin assembly. The coaxial hairpins shown here are suitable for studying $\Delta m_F = \pm 1$ transitions.

for the best impedance match by twisting the coupler from outside the vacuum system.

Most of the experimental work was done using the cavity shown in Fig. III-4. The rf magnetic field lines inside the cavity are concentric with the cylinder axis. H_{rf} is zero at the center and rises to a maximum value about three-quarters of the way out to the wall. At the wall, H_{rf} has a non-zero value. The beam experiences an oscillating rf magnetic field that is perpendicular to the static field H_0. The electric field and vector potential are directed parallel to the cavity axis and perpendicular to the faces. The beam hence experiences an oscillating rf electric field and vector potential that are parallel to the static magnetic field H_0.

3. Ramsey Pattern: Fields oscillating in phase and at a frequency equal to the transition frequency of interest are established in the two hairpins which are separated by a distance of six inches (center to center). The separated hairpin technique used here and developed by Ramsey[3] has become standard for precision atomic beam work and will not be discussed in detail. The method has two features which are particularly important for this experiment.

The first important feature of the technique is that it produces narrower linewidths than one using only a single hairpin of the same size. The signal observed at the detector for a constant static magnetic field, constant power input to the cavity but varying hairpin frequency is shown in Fig. III-7. This is also a plot of transition probability versus frequency. The pedestal is the resonance that

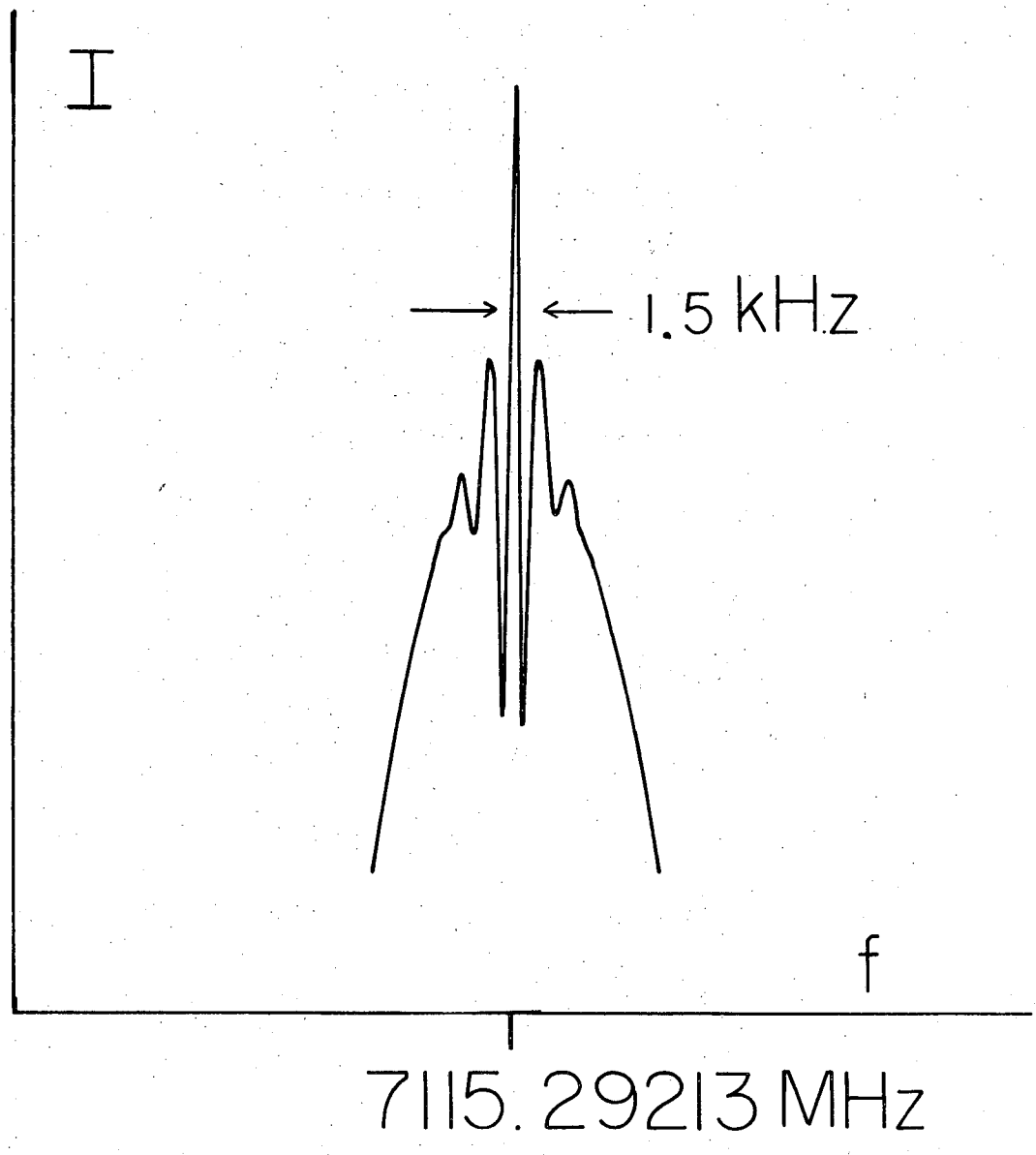

Fig. III-7. Chart recorder tracing of beam intensity versus hairpin frequency (Ramsey pattern).

would be obtained using a single hairpin while the (Ramsey) pattern at the top is due to the interference of the two hairpins. The base line has been suppressed. The full width at half-maximum of the single hairpin resonance is typically 20 to 30 kHz, while the width of the central peak of the Ramsey pattern is a factor of 10 smaller.

The second important feature of the Ramsey technique is that the transition probability is a maximum when the hairpin frequency equals the average transition frequency in the region between the hairpins. Thus the technique is sensitive to changes in transition frequency caused by perturbations introduced in the intermediate region.

4. C-Field Stabilization: The constant magnetic field H_0 in the C region is provided by a 12-in. electromagnet (Varian Associates V4012A) powered by a constant-current supply (Varian V2100) which is stable to one part in 10^5. Additional stability is produced by a proton nuclear-magnetic-resonance field controller (Harvey-Wells FC502). The marginal oscillator used to generate the proton NMR frequency was coupled to a highly stable oscillator (Schomandl ND5) to prevent drift. The complete field control circuit is shown schematically in Fig. III-8. With the use of this control circuit the field remained locked for as long as several days.

5. Radio-Frequency Equipment:

a. Transition Frequencies: Microwave signals oscillating at cesium transition frequencies are generated by a phase locked, continuously operating klystron (Sperry model 2K44 or Varian model X13 or X13B) and fed to the separated hairpins as illustrated in Fig. III-9.

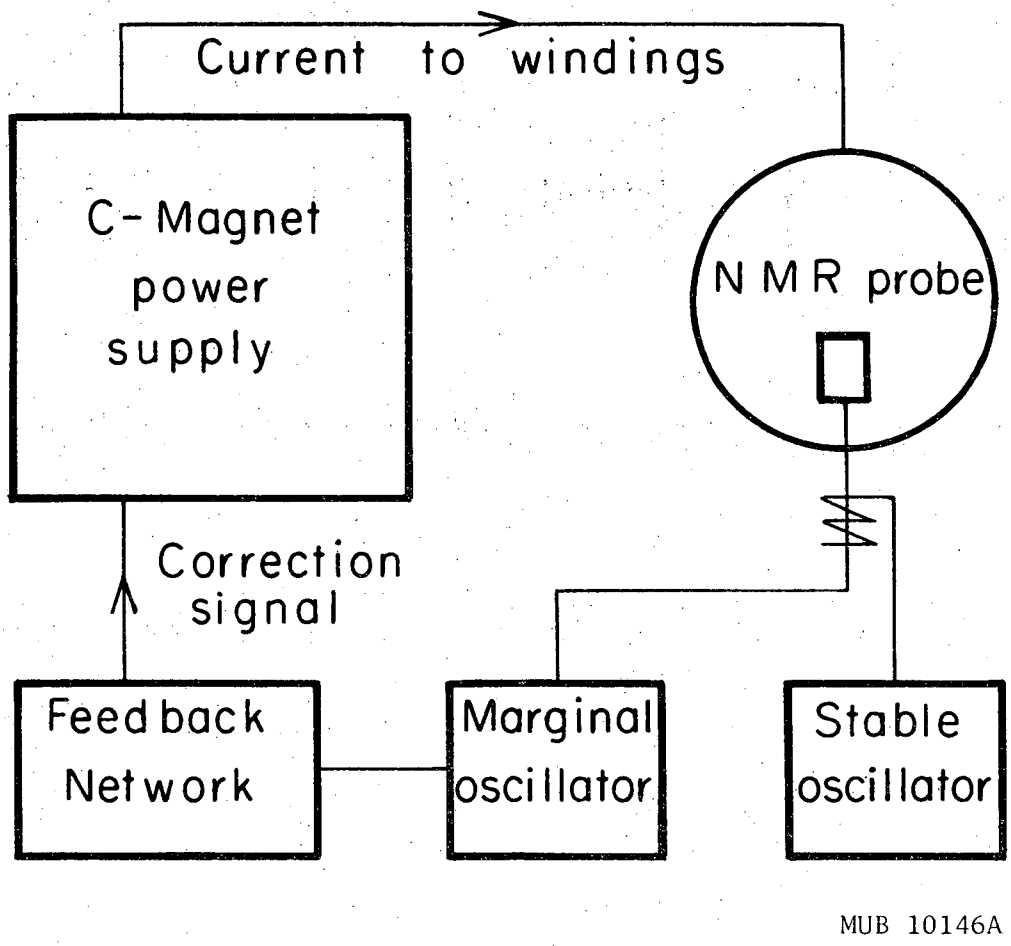

Fig. III-8. NMR magnetic field control unit.

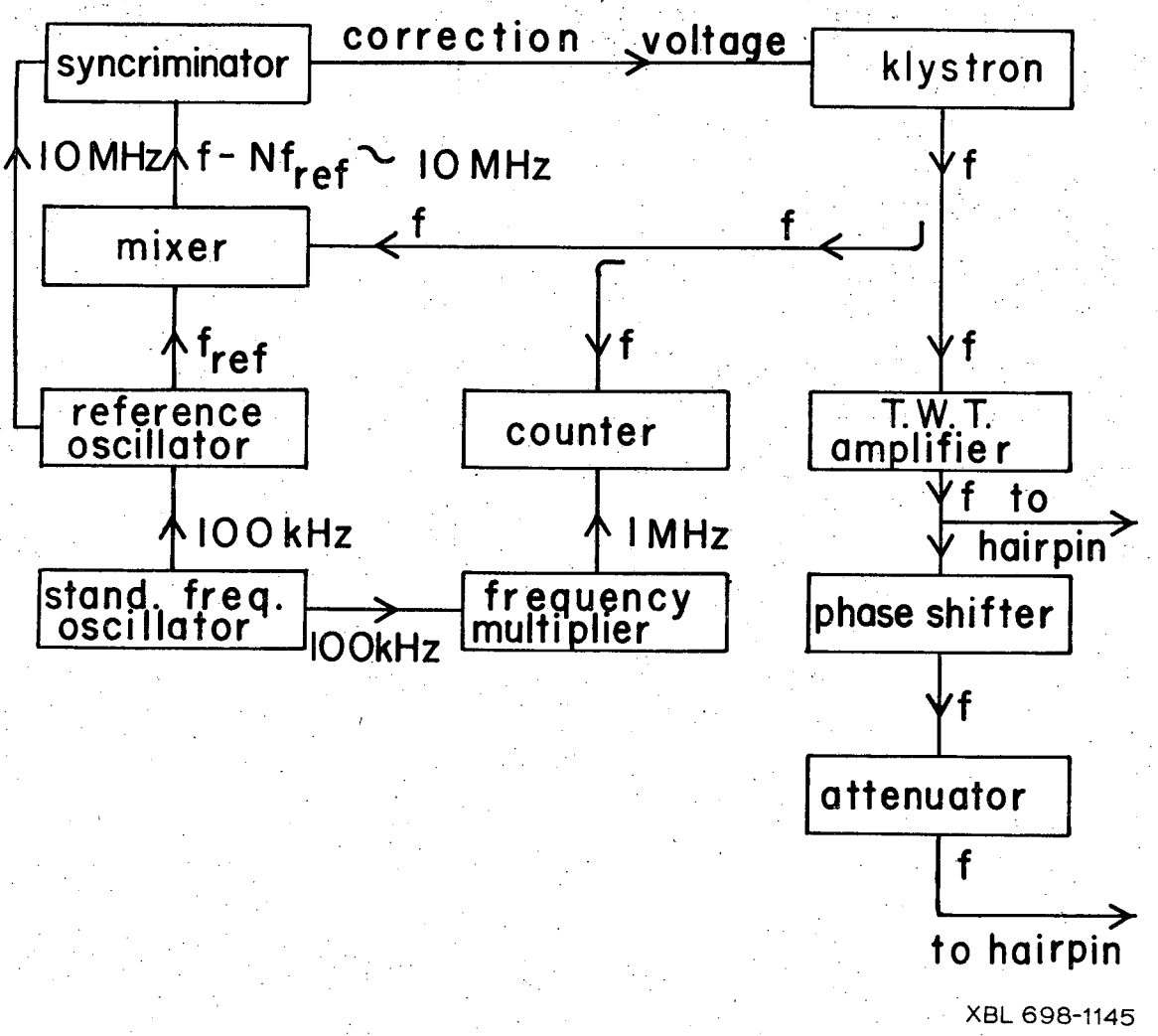

Fig. III-9. Block diagram of hairpin circuit.

A very stable reference oscillator (Schomandl FD3) provides a fundamental frequency between 300 MHz and 1000 MHz. This frequency synthesizer is adjusted to generate an output frequency $f_{ref} = (f - 10\ MHz)/N$, where f is the desired klystron output frequency, and N is an integer, usually 8 or 10. The phase of the beat frequency $f - Nf_{ref} \approx 10$ MHz produced in the mixer is compared with that of a 10 MHz if reference which is also produced by the reference oscillator. This comparison is made by a Schomandl FDS-3 syncriminator which applies a correction voltage to the reflector of the klystron that is proportional to the cosine of the phase difference between the beat (if) signal and the if reference signal.

Klystron frequencies are counted directly with a Hewlett-Packard 5245L counter using the 5255A frequency converter which is capable of counting frequencies between 3.0 and 12.4 GHz. Both the reference oscillator and the counter are referred to the same 100 kHz quartz crystal oscillator (James Knight FS1100T) which is, in turn, continuously compared with the 60 kHz standard frequency broadcast by the National Bureau of Standards' station WWVB, Fort Collins, Colorado. Because of the high stability of the 100 kHz reference, the precision of frequency measurements was determined by the uncertainty of ±1 in the last place of the counter display.

A traveling wave tube amplifier (Hewlett-Packard model 493A or 495A) boosts the klystron signal which is then divided, one-half being sent directly to one hairpin, and the other half being sent through a phase shifter (AMCI Line Stretcher model 3807N) and variable attenuator to the other hairpin.

The attenuator allows one to equalize the rf field amplitudes in the two hairpins. The phase shifter provides a way of equalizing the phase of the signals reaching the hairpins by changing the electrical length of the transmission line leading to one of them. The two signals are judged to be in phase when a symmetrical Ramsey pattern is obtained (see Fig. III-7).

b. Magnetron-Cavity Circuit: The circuit used to power the cavity is shown schematically in Fig. III-10. The signal from an isolated continuously operating magnetron (Raytheon QK60) can be fed either to the cavity or to a dummy load (Narda model 369NM) capable of absorbing 175 W average power. Both input and return power are sampled with a 20 db dual directional coupler (Narda model 3022) and measured with the same power meter (General Microwave model 454AR). The magnetron frequency is counted directly with a Hewlett-Packard 5245L counter using a 5254A frequency converter.

Insertion losses of all circuit components (including cables) were measured, so that the actual power absorbed by the cavity could be determined from power meter readings of input and return power. These calibrations agreed with manufacturers' specifications when given. Assuming that these insertion losses are known to within ±0.1 db, the input power P_{in} can be determined from the power meter reading P_{meas}:

$$P_{in} = 0.95 \pm .03 \times 10^4 \, P_{meas} \quad .$$

When making measurements of the cavity resonance profile, the power divider was removed, and a sample of the signal taken directly

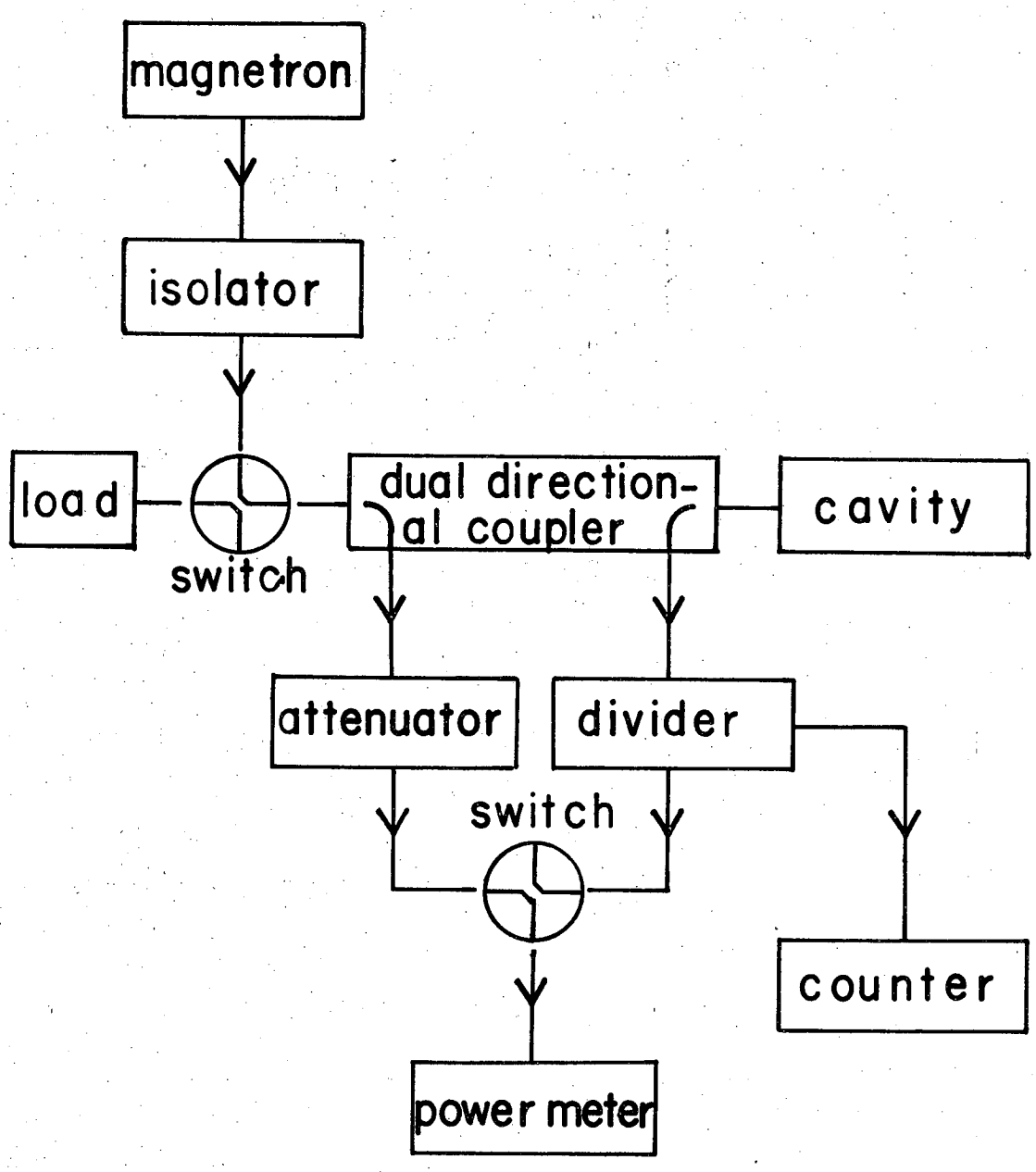

Fig. III-10. Block diagram of cavity circuit.

after the isolator was counted. Figure III-11 is a plot of the ratio of reflected power to incident power versus frequency for the TM_{010} cavity used in Runs 11 through 25. The points represent measurements while the curve is an inverted Lorentz profile characterized by

$$\nu_o = 2921.2 \text{ MHz}$$

$$Q = 4200 \pm 200$$

$$\text{Base line: } 0.77 \pm 0.01$$

At resonance the return power was less than 0.1% of the incident power. The displaced base line is due to constant circuit losses and suggests that the power absorbed at resonance is 77% of the incident power. The calibrated circuit losses gave the result $P_{in} = 0.95 \pm .03 \times 10^4 \, P_{meas}$, so the actual absorbed power is 77% of this, or

$$P_{abs} = 0.73 \pm .02 \times 10^4 \, P_{meas} \quad .$$

Thus a power meter reading of 1 mW corresponds to an absorbed power of $7.3 \pm .2$ W.

6. Cavity Design: The effective vector potential experienced by an atomic beam that traverses a TM_{010} cylindrical cavity along a diameter midway between the ends is given by (see Appendix B)

$$A = -i|A| \, e^{-i\omega t}$$

where

$$|A|^2 = 0.455 \left(\frac{c}{\omega}\right)^2 E_0^2$$

and

$$E_0^2 = 203 \frac{PQ\nu_o}{\ell c^2} \quad .$$

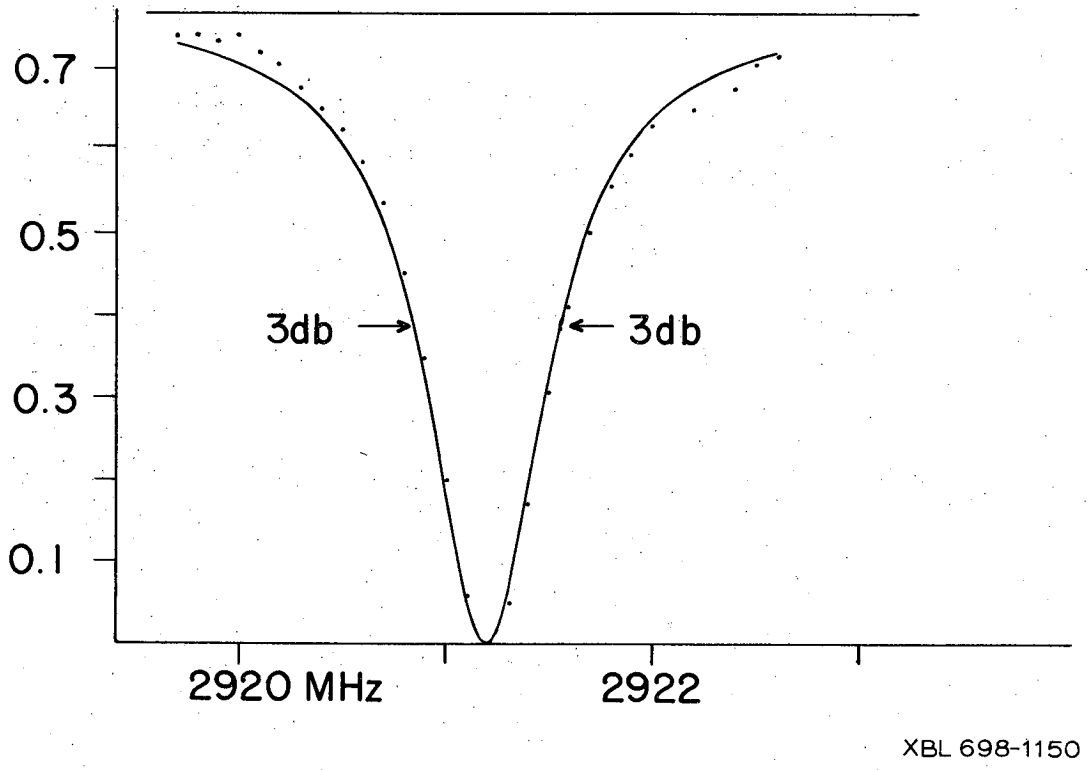

Fig. III-11. TM_{010} cavity resonance (absorption) profile: Normalized reflected power versus frequency.

The square of the amplitude of the vector potential can be written

$$|A|^2 = 2.34 \frac{PQ}{\nu_o \ell}$$

where P is the power dissipated in the walls in erg/sec, ν_o is the resonant frequency in Hz, ℓ is the length in cm, and Q is the unloaded Q. A more practical expression is

$$|A|^2 = 2.34 \times 10^{-2} \frac{PQ}{\nu_o \ell}$$

where P is in Watt, ν_o in GHz, ℓ in cm and $|A|^2$ in esu (erg/cm). The electron relative mass shift is assumed to be

$$\frac{\delta m}{m} = \frac{1}{2} \frac{e^2 |A|^2}{(mc^2)^2} = \frac{1}{2} \frac{r_o}{mc^2} |A|^2$$

or

$$\frac{\delta m}{m} = 4.03 \times 10^{-9} \frac{PQ}{\nu_o \ell} \quad .$$

Thus a relative mass shift of 4×10^{-6} can be induced when 1 W of power is absorbed in a cavity of length 1 cm, resonant frequency 1 GHz and Q 1000.

The above formula suggests the following design criteria for obtaining a maximum mass shift: i) use as low a frequency as possible, ii) use as short a cavity as possible, iii) use as much power as possible, and iv) maximize Q by choosing a high conductivity metal from which to fashion the cavity. These criteria are not all independent. For example, in the TM_{010} mode the radius determines the resonant frequency[5] so that a low ν_o implies a large radius. A large radius R and short length ℓ produce a large ratio R/ℓ. However, a

large value of R/ℓ yields a small Q.[6] With these considerations in mind it was decided to build a silver-plated TM_{010} cavity 1.91 cm long, resonant at about 3 GHz. The parameters for the actual cavity were

$$\nu_o = 2.921 \text{ GHz}$$
$$\ell = 1.91 \text{ cm}$$
$$Q = 4200 \pm 200 \quad .$$

Thus, for one watt of absorbed power, the expected relative mass shift is

$$\frac{\delta m}{m} \simeq 3 \times 10^{-6} \quad .$$

D. Experimental Procedure

A typical run proceeded as follows: Once the apparatus was evacuated, the magnetic field set and locked, the radiofrequency equipment set up, and a nominal beam intensity achieved, the phase shifter was adjusted to give a symmetrical Ramsey pattern. The magnetron was then set for maximum output and tuned to the cavity resonant frequency by adjusting the tuning knob for minimum return power. After several minutes the water-cooled cavity came to equilibrium, and the return power was steady and less than 1% of the input power.

A measurement was then made of the position of the center of the central peak in the Ramsey pattern. This was done by averaging frequency readings taken at two or three positions symmetrically located on each side of the central peak. Hence, four or six frequency measurements, when averaged, gave one value for the center frequency. This procedure was performed ten times and the average of the ten

center frequencies so measured was taken to be the best value for the transition frequency. Without changing the cavity input power, the transition frequency of the other member of the doublet was then determined in the same way. The cavity power was then decreased, and, after equilibrium was achieved, the two frequencies were again measured. In this way the transition frequency was measured for five values of cavity power, including zero power. The five measurements of each transition frequency were then fit by a least squares procedure to a straight line[7] with each point weighted in inverse proportion to its standard deviation.

IV. EXPERIMENTAL RESULTS

A. Introduction

The results of twenty-seven measurements of ^{133}Cs hfs transition frequency shifts induced by the fields of a high-Q microwave cavity reveal no evidence of an electron mass shift. The measurements were sensitive enough to detect the Bloch-Siegert effect which is three orders of magnitude smaller than the expected mass shift effect. The negative result is in agreement with the conclusion of Chapter II that the second order effects of the plane wave field cancel one another.

B. Presentation of Data

Figures IV-1, IV-2 and IV-3 are representative plots of transition frequency versus cavity power for the three field-independent doublets studied. Neither the mass shift effect nor the Bloch-Siegert effect are strongly dependent upon the static magnetic field H_0, so the field values quoted are only nominal, i.e., within a couple of gauss of the desired field-independent points. Each of the three figures summarizes the results of one run and indicates how well the data fit straight lines.

Table IV-1 summarizes the results of runs made with a TM_{010} cavity resonant at 2.921 GHz. The designations a_1, a_2, etc. refer to Table III-1 and Fig. III-1. The shifts quoted are normalized to a power meter reading of 0.1 mW. Errors quoted for individual measurements are one mean standard deviation of the fitted slopes and indicate the precision

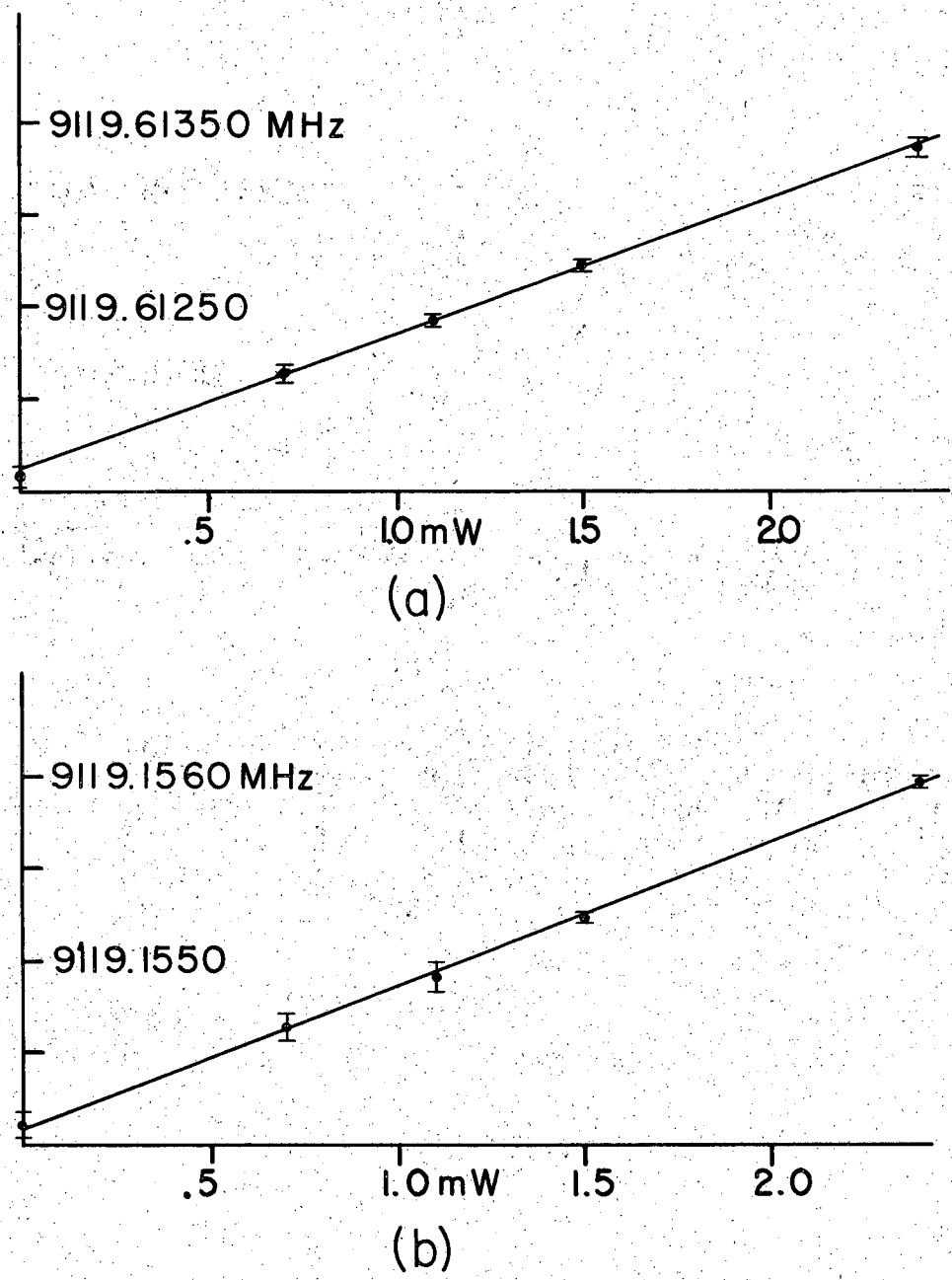

XBL 698-1151

Fig. IV-1. Transition frequency versus power meter reading. 415 G doublet (Run 21). Cavity frequency = 2921 MHz. (a). (4,-1)↔(3,0). Slope = 73(3) Hz/0.1 mW, intercept = 9119.61161(4) MHz. (b). (4,0)↔(3,-1). Slope = 77(3) Hz/0.1 mW, intercept = 9119.55409(5) MHz. Error bars represent one mean standard deviation.

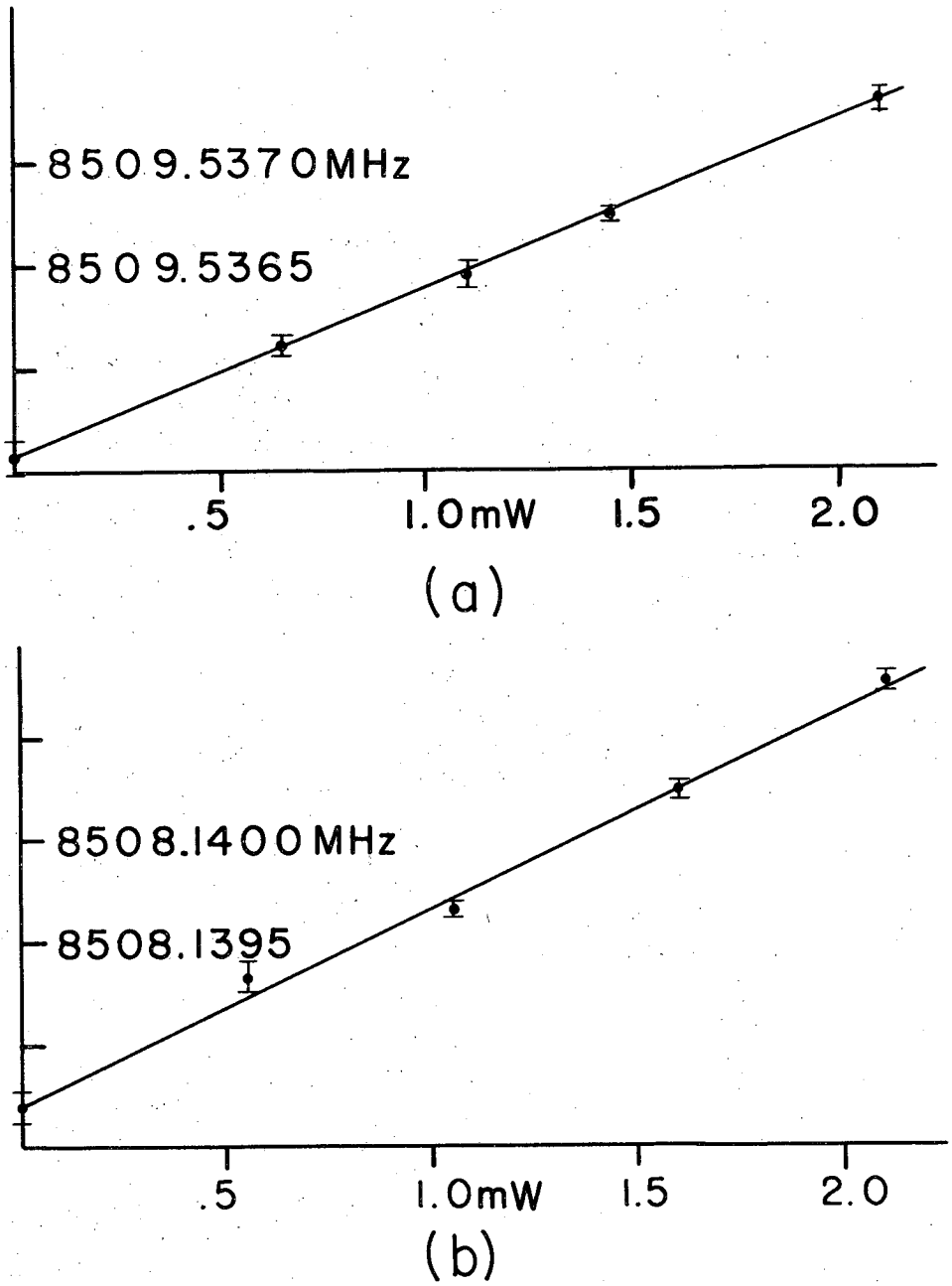

XBL 698-1152

Fig. IV-2. Transition frequency versus power meter reading. 1250 G doublet (Run 18). Cavity frequency = 2921 MHz. (a). $(4,-2)\leftrightarrow(3,-1)$. Slope = 82(4) Hz/0.1 mW, intercept = 8509,53557(6) MHz. (b). $(4,-1)\leftrightarrow(3,-2)$. Slope = 96(3) Hz/0.1 mW, intercept = 8508.13870(6) MHz. Error bars represent one mean standard deviation.

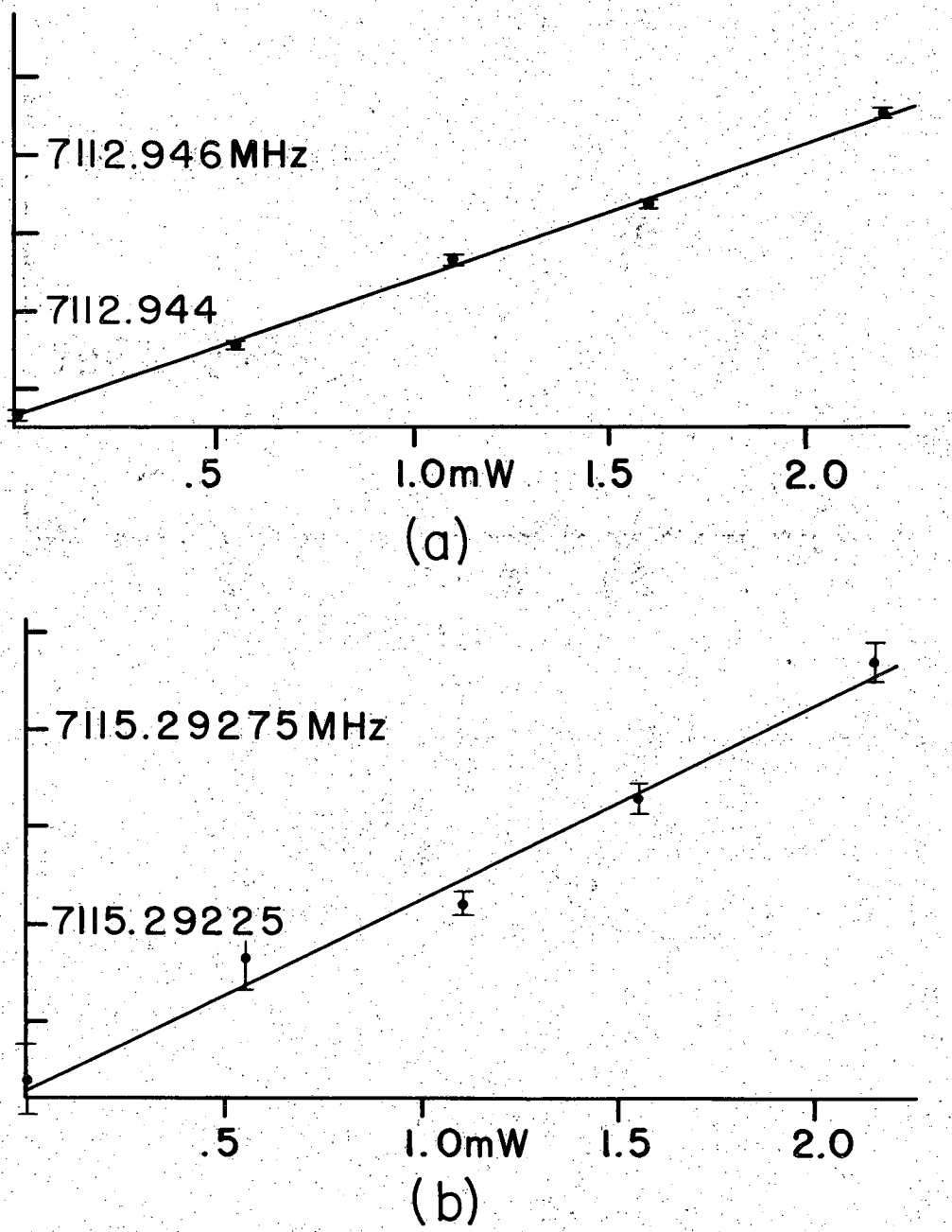

XBL 698-1153

Fig. IV-3. Transition frequency versus power meter reading. 2100 G doublet (Run 13). Cavity frequency = 2921 MHz. (a). $(4,-2)\leftrightarrow(3,-3)$. Slope = 174(2) Hz/0.1 mW, intercept = 7112.94264(2) MHz. (b). $(4,-3)\leftrightarrow(3,-2)$. Slope = 49(4) Hz/0.1 mW, intercept = 7115.29182(6) MHz. Error bars represent one mean standard deviation.

to which frequency measurements were made. The errors quoted for the averages are due to the spread of results from different runs and indicate the reproducibility of the measurements.

The results of some earlier exploratory runs (Runs 1 through 10), made with a more primitive cavity and each studying only one transition, are not included here. Problems with drifting magnetron power, drifting C-field, and insufficient beam intensity made their results insufficiently reproducible to merit comparison with later runs.

C. Interpretation of Measured Shifts

Three corrections have to be made to the raw data presented in Table IV-1 before it can be interpreted. The first correction is merely the change in units from mW to Watt. As discussed in Chapter III (Sec. C-5b), a power meter reading of 0.1 mW corresponds to 0.73 ±.02 W absorbed in the cavity. Each average shift must, therefore, be divided by 0.73 to get the actual shift in Hz/W .

Whenever the applied perturbation does not act over the entire distance between the separated hairpins, the measured shifts must be multiplied by the filling factor L/D where D is the length of the interaction region (cavity diameter), and L is the separation between the hairpins. This correction is necessary because the Ramsey technique samples the average transition frequency between the hairpins, and therefore the measured frequency is an average of the (perturbed) transition frequency when the atom is inside the cavity and the (unperturbed) transition frequency when the atom is between the hairpins but outside the cavity.

Table IV-1. DATA SUMMARY - Shifts Listed Here are Normalized to a Power Meter Reading of 0.1 mW

A-415 Gauss Doublet

Run No.	a_1 Shift	a_2 Shift
21	73±3 Hz	77±3 Hz
22	70±3	65±4
23	78±1	72±1
24	79±1	85±2
Average	75±4	75±7

B-1250 Gauss Doublet

Run No.	b_1 Shift	b_2 Shift
16	-----	92±4 Hz
17	80±3 Hz	97±2
18	82±4	96±3
19	86±3	92±3
20	89±3	89±2
Average	84±4	93±3

C-2100 Gauss Doublet

Run No.	c_1 Shift	c_2 Shift
11	46±1 Hz	165±2 Hz
12	40±3	177±3
13	49±4	174±2
14	49±2	146±3
25	46±1	186±1
Average	46±3	170±22

The third correction is an additive one. Whenever the average energy level separation of an atom in the region between the hairpins is not equal to the energy level separation in the hairpins, the peak frequency is shifted by an amount[1,2] $1.2 \frac{\ell}{L} \Delta\omega$ where $\Delta\omega$ is the difference between the transition frequency in the hairpins and the average transition frequency in the intermediate region, ℓ is the length of the beam path in a hairpin and L is the length of the intermediate region. The total correction to be applied to the averages S_{meas} given in Table IV-1 is

$$S_{obs} = S_{meas} \frac{L}{D} \frac{1}{0.73} \left(1 - 1.2 \frac{\ell}{L}\right)$$

$$S_{obs} = 2.05 \pm .04 \; S_{meas} \quad .$$

The observed shift can also be written in Hz/G^2 by using the conversion (Appendix B):

$$1 \; W \leftrightarrow 3.10 \pm .14 \; G^2 \quad .$$

When these corrections are made to the average frequency shifts given in Table IV-1, the results listed in Table IV-2 are obtained. The observed shifts (S_{obs}) are given in both Hz/W and Hz/G^2 for comparison with the expected mass shift effect (S_{ms}) and Bloch-Siegert effect (S_{B-S}). In addition to the discrepancy in absolute size, more than two orders of magnitude, between the observed shifts and those expected due to an electron mass shift, there is also a striking discrepancy in the relative size of the shifts of the 2100 G transitions c_1 and c_2. If these shifts were due to an increase in the electron

Table IV-2.

Comparison of Observed Shifts (S_{obs}) with Mass Shift Effect (S_{ms}) and Bloch-Siegert Effect (S_{B-S})

Transition	Frequency (MHz)	S_{ms} (Hz/watt)	S_{obs} (Hz/watt)	S_{obs} (Hz/gauss^2)	S_{B-S} (Hz/gauss^2)
a_1	9119.6	55 ±4 x 10^3	154 ±9	50 ±3	60
a_2	9119.1	55 ±4	154 ±15	50 ±3	62
b_1	8509.5	52 ±4	172 ±9	56 ±3	61
b_2	8508.1	52 ±4	191 ±7	62 ±4	72
c_1	7115.3	43 ±3	94 ±6	30 ±2	38
c_2	7112.9	43 ±3	349 ±46	113 ±8	150

mass, the two should be equal (to within a few percent), whereas they differ by a factor of about 3.7 .

On the other hand, there is good agreement, between the six observed shifts and those expected on the basis of a many-level Bloch-Siegert effect. This effect amounts to a shift in the maximum transition probability (i.e., the central peak of the Ramsey pattern) due to the presence of a non-resonant perturbation. Evidently, the rf magnetic field in the cavity has been slightly over estimated, causing the calculated Bloch-Siegert shifts to be somewhat larger than the listed measurements. The relative sizes of the six measurements, however, agree completely, within experimental error, with the calculated Bloch-Siegert shifts.

An oscillating magnetic field H_{rf}, oriented at right angles to a given C-field H_0, shifts a given magnetic dipole transition frequency f by[3]

$$\Delta f = \left(\frac{\mu_o}{h} g_J \frac{H_{rf}}{2}\right)^2 \sum_j \sum_i \left\{ \frac{|\langle i|J_x|1\rangle|^2}{\left(\frac{W_i - W_1}{h} - \nu_j\right)} + \frac{|\langle 2|J_x|i\rangle|^2}{\left(\frac{W_2 - W_i}{h} - \nu_j\right)} \right\}$$

where $(W_2-W_1)/h$ is the transition frequency under study. The index j takes on two values corresponding to $\nu_j = \pm\nu_o$, the frequency of the non-resonant perturbation. The index i runs through all the states that can be reached by a π-type transition from either the initial or the final state. This many-level Bloch-Siegert effect is seen to be proportional to the square of the rf magnetic field and hence is a linear function of power.

Because of the resonance denominators, remotely probable transitions which lie close to the non-resonant perturbing frequency (i.e., the cavity frequency) will influence the total transition probability more than those lying farther away. Figure IV-4 illustrates, for the 2100 G doublet, what transitions can be induced (with remote probability) by the cavity rf magnetic field. The left-most line in each case is the transition under study (i.e., the 7.1 GHz transition). The other five in each case serve to distort the total transition probability unequally for the two transitions. The inequality comes from about the unequal influences of the $(3,-2) \leftrightarrow (3,-1)$ transition on the left and the $(4,-4) \leftrightarrow (3,-3)$ transition on the right due to their unequal frequencies.

Perhaps the quickest way to test whether one is observing the Bloch-Siegert effect or the mass-shift effect is to choose a cavity mode for which a mass shift theory predicts large, positive and equal frequency shifts for the two members of a π doublet, while the expected Bloch-Siegert shifts are small, negative and unequal. Such is the case for the 2100 G doublet when the cavity frequency is 7930 MHz, and H_{rf} is perpendicular to H_0. Seven runs were made at this frequency using a TM_{210} cavity powered by a Litton L3508 mechanically-tuned magnetron. Figure IV-5 is a plot of transition frequency versus power for one such run. The frequency shifts are clearly negative and unequal. The results of these runs reinforce the conclusion drawn from Table IV-2; namely, that no shifts are observed which cannot be interpreted as Bloch-Siegert shifts.

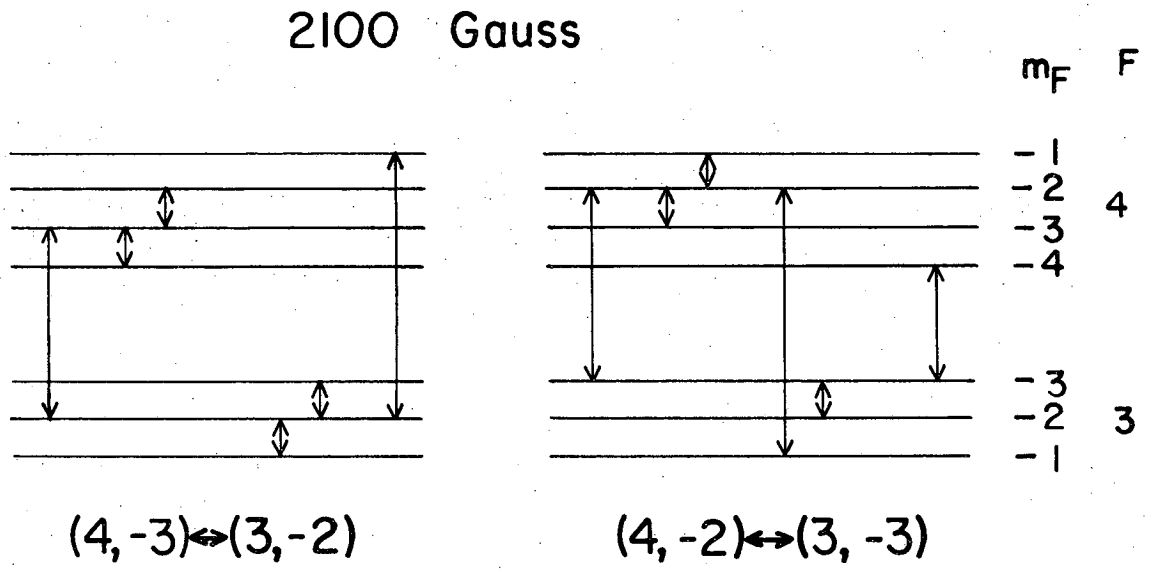

Fig. IV-4. Remotely probable transitions induced by non-resonant rf magnetic field oriented at right angles to static field H_0.

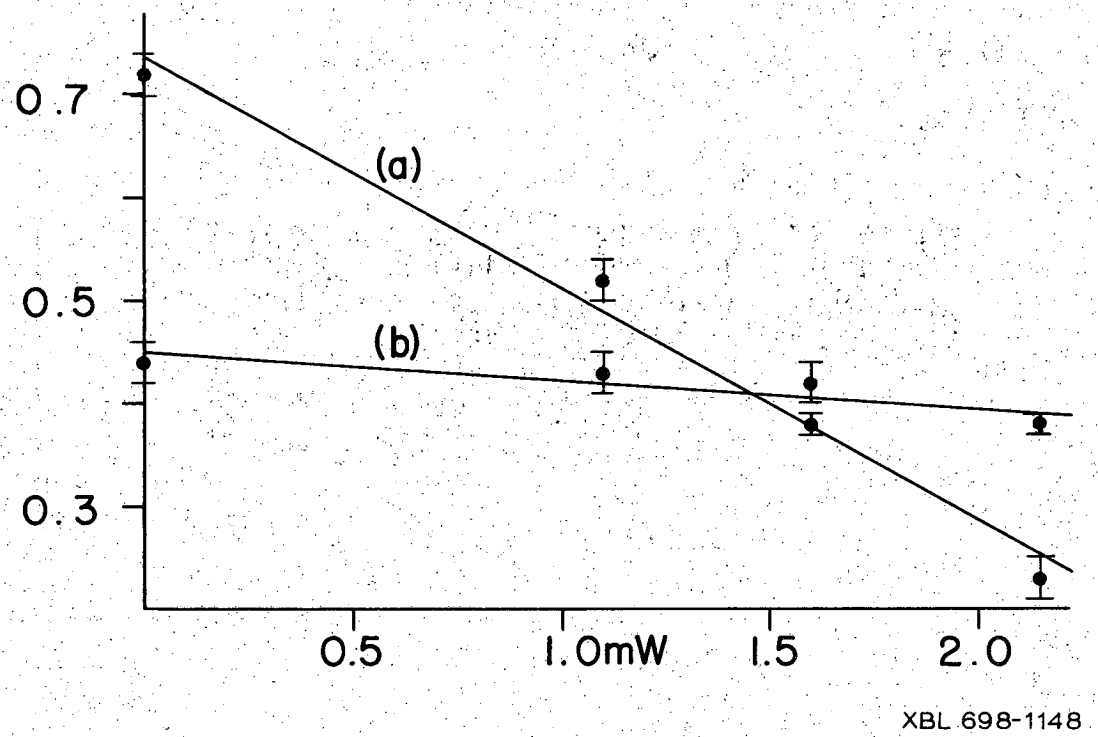

Fig. IV-5. Transition frequency versus power meter reading. 2100 gauss doublet (Run 28). Cavity frequency = 7930 MHz. (a). $(4,-2)\leftrightarrow(3,-3)$. Slope = -22.5±1.2 Hz/0.1mW, ordinate = f-7112,942.0 kHz. (b). $(4,-3)\leftrightarrow(3,-2)$. Slope = -2.8±1.0 Hz/0.1 mW, ordinate = f-7115,291.0 kHz. Error bars represent one mean standard deviation.

D. Conclusion: Why the Mass Shift Effect Was Not Observed

Arguments similar to those used in Chapter II. Section E can be invoked to explain the negative results summarized above. Return to the point where the mass shift was introduced [Eq. II-7]:

$$(E-e\phi)^2\psi = [(\vec{p} - \frac{e}{c}\vec{A}_s)^2 + (mc^2)^2 + e^2a^2 + ec\hbar(\vec{\sigma}\cdot\vec{B} - i\vec{\alpha}\cdot\vec{E})]$$

where the time-dependent terms have been dropped. There are three ways in which the constant term e^2a^2 my be handled: i) combine e^2a^2 with $(mc^2)^2$ to get a renormalized mass as was done in Chapter II, ii) combine e^2a^2 with $W = E - mc^2$ and get the same shift for all energy levels, or iii) leave the term in the equation until after the non-relativistic approximation has been obtained, treat it by perturbation theory, and get an equal shift of all energy levels. Alternatives ii) and iii) are equivalent to order $1/m^2$, i.e., when the relativistic term $\frac{1}{2mc^2}(W-e\phi)^2$ is neglected.

The oscillating fields experienced by a beam atom traversing a diameter of a TM_{010} cavity are roughly similar to those of a linearly polarized plane wave which can be represented by

$$\vec{A} = \hat{\varepsilon}ae^{i(kx-\omega t)}$$

$$A^2 = \frac{a^2}{2}(1 + \cos 2(kx-\omega t))$$

where $\hat{\varepsilon}$ is the (real) polarization vector. If the e^2A^2 term is carried through to the non-relativistic approximation, it becomes

$$\frac{e^2A^2}{2mc^2} = \frac{e^2a^2}{4mc^2} + \frac{e^2a^2}{8mc^2}\left(e^{2ikx} + e^{-2ikx}\right)$$

where the $e^{\pm 2i\omega t}$ factors in the cosine have been set to their zeroth order values, namely, unity. When the previously neglected $\frac{-e}{mc}\vec{A}\cdot\vec{p}$ term is treated in second order perturbation theory and the $e^2a^2/2mc^2$ term is treated in first order perturbation theory one obtains, with the aid of [Eq. (II-41)],

$$\frac{-e}{2mc}\vec{A}\cdot\vec{p} \rightarrow \frac{-e^2a^2}{2mc^2}$$

$$\frac{e^2A^2}{2mc^2} \rightarrow \frac{e^2a^2}{4mc^2} + \frac{e^2a^2}{8mc^2}\cdot 2 = \frac{e^2a^2}{2mc^2}$$

i.e., the (first order) energy shift due to the mass renormalization term is exactly canceled by the (second order) energy shift due to the $\vec{A}\cdot\vec{p}$ term. In the light of the negative experimental results, it appears that the proper way to treat the e^2A^2 term is by perturbation theory, and not to consider it as an electron mass renormalization.

ACKNOWLEDGMENTS

Several persons have made significant contributions to this work. Professors Charles Schwartz, P. G. H. Sandars and W. A. Nierenberg each suggested independently that the mass-shift effect probably would not occur for hydrogen-like atoms because the e^2A^2 term would be canceled by the $\vec{A}\cdot\vec{p}$ term in second-order perturbation theory. It was Professor Schwartz who pointed out an error in my argument of Chapter I, Sec. E which, when corrected, led to the anticipated cancellation.

Dr. Charles Johnson was my partner on this experiment. His experience with microwave cavities and electronic circuits helped keep the work progressing swiftly. It was he who suggested that the shifts we did observe could probably be understood as a multi-level Bloch-Siegert effect. Professor Vernon Ehlers, in addition to proposing the experiment, spent a generous portion of one summer helping to get the beam machine and magnetic field control circuit in proper working order. Thanks are also due to Mr. Rudy Johnson and Mr. Douglas MacDonald for aid in designing the cavity and hairpin assembly, and to Mr. Walter Brown for machining them.

I am especially grateful to Professor Howard Shugart for his leadership and advice. As head of the Berkeley Atomic Beam Group, his constant enthusiasm and encouragement helped build my self-confidence as a physicist. There is not a single person in the atomic beam group who at one time or another has not provided me with useful assistance when needed, and it has been an inspiration to work on such a team.

In particular, I appreciate the hard work of Mrs. Julia Taylor and Miss Nadine Kamada who have done such a beautiful job in typing this thesis.

I am deeply grateful for the patience, understanding and confidence of my wife Lisa who spent many long evenings and weekends alone while I was doing physics, and who, without complaint, subsists on the half of me that is not wedded to my work.

This work was supported by the U. S. Atomic Energy Commission.

APPENDICES

A. Quadratic Dirac Equation

I. Introduction: This appendix contains detailed calculations which supplement the theory given in Chapter II for an electron in an electromagnetic field. The quadratic (or second order) Dirac equation is obtained from the linear (or first order) Dirac equation.

A. Metric: The signature of the metric is chosen to be (1, -1, -1, -1) so that the product of two four-vectors A and B is

$$A \cdot B = (A_o, \vec{A}) \cdot (B_o, \vec{B}) = A_o B_o - \vec{A} \cdot \vec{B} \quad .$$

B. Representation of γ Matrices:[1] The following representation will be used:

$$\gamma_o = \begin{pmatrix} I & 0 \\ 0 & -I \end{pmatrix} = \beta \tag{A1}$$

$$\vec{\gamma} = \begin{pmatrix} 0 & \vec{\sigma} \\ -\vec{\sigma} & 0 \end{pmatrix} \tag{A2}$$

$$\vec{\alpha} = \begin{pmatrix} 0 & \vec{\sigma} \\ \vec{\sigma} & 0 \end{pmatrix} = \gamma_o \vec{\gamma} \quad , \tag{A3}$$

where

$$\vec{\sigma} = \begin{pmatrix} 0 & 1 \\ 1 & 0 \end{pmatrix} \hat{x} + \begin{pmatrix} 0 & -i \\ i & 0 \end{pmatrix} \hat{y} + \begin{pmatrix} 1 & 0 \\ 0 & -1 \end{pmatrix} \hat{z}$$

and

$$I = \begin{pmatrix} 1 & 0 \\ 0 & 1 \end{pmatrix} \quad .$$

II. Construction of the Quadratic Equation: The relativistic wave equation for an electron in an electromagnetic field may be written

in the following co-variant form:[2]

$$[c\gamma\cdot(p - \frac{e}{c}A) - mc^2]\psi = 0 \quad , \tag{A4}$$

where $e = -4.803 \times 10^{-10}$ esu is the electron charge and mc^2 is its rest energy. The energy-momentum four-vector

$$p = (\frac{E}{c}, \vec{p}) = i\hbar\Box = (i\hbar\frac{1}{c}\frac{\partial}{\partial t}, -i\hbar\nabla)$$

is composed of the total energy E and the total linear momentum $\vec{p}$, and the four-vector potential

$$A = (\phi, \vec{A})$$

is composed of the electrostatic scalar potential ϕ and the magnetic vector potential $\vec{A}$.

Equation (A4) can readily be converted to the more familiar form involving $\vec{\alpha}$ and β. After multiplying by $-\gamma_o$ on the left, one has

$$[-c\gamma_o\gamma_o(p_o - \frac{e}{c}A_o) + c\gamma_o\vec{\gamma}\cdot(\vec{p} - \frac{e}{c}\vec{A}) + \gamma_o mc^2]\psi = 0$$

$$[-c(\frac{E}{c} - \frac{e}{c}\phi) + c\vec{\alpha}\cdot(\vec{p} - \frac{e}{c}\vec{A}) + \beta mc^2]\psi = 0$$

or,

$$(c\vec{\alpha}\cdot\vec{\pi} + e\phi + \beta mc^2)\psi = E\psi \tag{A5}$$

where

$$\vec{\pi} \equiv \vec{p} - \frac{e}{c}\vec{A} \tag{A6}$$

is known as the kinetic momentum.

By analogy with Eq. (A6) the kinetic four momentum π is defined as

$$\pi = p - \frac{e}{c} A \quad .$$

Define

$$\not{\pi} \equiv \gamma \cdot \pi \tag{A7}$$

so that Eq. (A4) becomes

$$(c\not{\pi} - mc^2)\psi = 0 \quad ;$$

multiply by $c\not{\pi} + mc^2$ to get

$$(c\not{\pi} + mc^2)(c\not{\pi} - mc^2)\psi = 0$$

or

$$[c^2 \not{\pi} \cdot \not{\pi} - (mc^2)^2]\psi = 0 \tag{A8}$$

Equation (A8) is a second order differential equation for the four component spinor wave function ψ. The remainder of this appendix is devoted to evaluating the product $\not{\pi} \cdot \not{\pi}$ in terms of the electric and magnetic fields acting on the electron.

III. Evaluation of $\not{\pi} \cdot \not{\pi}$: In this section it is shown that

$$\not{\pi} \cdot \not{\pi} = \pi \cdot \pi + \frac{e\hbar}{c} (\vec{\sigma} \cdot \vec{B} - i\vec{\alpha} \cdot \vec{E}) \quad .$$

The proof of this identity is straightforward. Beginning with the definition of $\not{\pi}$ given by Eq. (A7), one can write

$$\not{\pi} \cdot \not{\pi} = (\gamma \cdot \pi)(\gamma \cdot \pi) = (\gamma_o \pi_o - \gamma \cdot \pi)(\gamma_o \pi_o - \gamma \cdot \pi) = \begin{pmatrix} \pi_o & -\vec{\sigma} \cdot \vec{\pi} \\ \vec{\sigma} \cdot \vec{\pi} & -\pi_o \end{pmatrix} \begin{pmatrix} \pi_o & -\vec{\sigma} \cdot \vec{\pi} \\ \vec{\sigma} \cdot \vec{\pi} & -\pi_o \end{pmatrix}$$

$$\not{\pi} \cdot \not{\pi} = [\pi_o \pi_o - (\vec{\sigma} \cdot \vec{\pi})(\vec{\sigma} \cdot \vec{\pi})] \begin{pmatrix} I & 0 \\ 0 & I \end{pmatrix} + [\vec{\pi}, \pi_o] \begin{pmatrix} 0 & \vec{\sigma} \\ \vec{\sigma} & 0 \end{pmatrix} \quad .$$

Apply the identity

$$(\vec{\sigma}\cdot\vec{A})(\vec{\sigma}\cdot\vec{B}) = \vec{A}\cdot\vec{B} + i\vec{\sigma}\cdot(\vec{A}\times\vec{B})$$

and the definition of $\vec{\alpha}$ given by Eq. (A3) to get

$$\not{\pi}\cdot\not{\pi} = \pi_o\pi_o - \vec{\pi}\cdot\vec{\pi} - i\vec{\sigma}\cdot(\vec{\pi}\times\vec{\pi}) + \vec{\alpha}\cdot[\vec{\pi},\pi_o]$$

or

$$\not{\pi}\cdot\not{\pi} = \pi\cdot\pi - i\vec{\sigma}\cdot(\vec{\pi}\times\vec{\pi}) + \vec{\alpha}\cdot[\vec{\pi},\pi_o] \quad . \tag{A9}$$

Consider the operator $\vec{\pi}\times\vec{\pi}$:

$$\vec{\pi}\times\vec{\pi}\psi = (\vec{p} - \frac{e}{c}\vec{A}) \times (\vec{p} - \frac{e}{c}\vec{A})\psi$$

$$= (-i\hbar\nabla - \frac{e}{c}\vec{A}) \times (-i\hbar\nabla - \frac{e}{c}\vec{A})\psi$$

$$= -\hbar^2\nabla\times\nabla\psi + i\hbar\frac{e}{c}\nabla\times\vec{A}\psi + i\hbar\frac{e}{c}\vec{A}\times\nabla\psi + \frac{e}{c}\vec{A}\times\vec{A}\psi \quad . \tag{A10}$$

Now, $\nabla\times\nabla\psi = 0$ because the curl of any gradient vanishes identically, and $\vec{A}\times\vec{A} = 0$ since $\vec{A}$ is parallel to itself. Furthermore,

$$\nabla\times(\vec{A}\psi) = -\vec{A}\times\nabla\psi + (\nabla\times\vec{A})\psi \quad ,$$

so that Eq. (A10) becomes

$$\vec{\pi}\times\vec{\pi}\psi = i\hbar\frac{e}{c}(\vec{\nabla}\times\vec{A})\psi = i\hbar\frac{e}{c}\vec{B}\psi \quad . \tag{A11}$$

Consider next the operator $[\vec{\pi},\pi_o]$:

$$[\vec{\pi},\pi_o]\psi = \left[-i\hbar\nabla - \frac{e}{c}\vec{A},\ \frac{i\hbar}{c}\frac{\partial}{\partial t} - \frac{e}{c}\phi\right]\psi$$

$$= i\hbar\frac{e}{c}\nabla(\phi\psi) - i\hbar\frac{e}{c}\phi\nabla\psi - \frac{ie\hbar}{c^2}\vec{A}\frac{\partial}{\partial t}\psi + \frac{i\hbar e}{c^2}\frac{\partial}{\partial t}(\vec{A}\psi)$$

$$= i\hbar \frac{e}{c} [(\nabla\phi)\psi + \phi\nabla\psi - \phi\nabla\psi] + i\hbar \frac{e}{c} \left[\frac{1}{c}\left(\frac{\partial}{\partial t}\vec{A}\right)\psi + \frac{\vec{A}}{c}\frac{\partial}{\partial t}\psi - \frac{\vec{A}}{c}\frac{\partial\psi}{\partial t}\right]$$

$$= i\frac{e\hbar}{c}\left(\frac{1}{c}\frac{\partial}{\partial t}\vec{A} + \nabla\phi\right)\psi$$

$$= -i\frac{e\hbar}{c}\vec{E}\,\psi$$

$$[\vec{\pi}, \pi_o] = -i\frac{e\hbar}{c}\vec{E} \quad . \tag{A12}$$

when Eqs. (A11) and (A12) are inserted into Eq. (A9), one finds the desired result:

$$\not{\pi}\cdot\not{\pi} = \pi\cdot\pi + \frac{e\hbar}{c}(\vec{\sigma}\cdot\vec{B} - i\vec{\alpha}\cdot\vec{E}) \quad . \tag{A13}$$

IV. The Quadratic Equation: When the expression for $\not{\pi}\cdot\not{\pi}$ derived in the preceeding section is inserted into Eq. (A8), one has

$$[c\pi\cdot c\pi - (mc^2)^2]\psi = -ec\hbar(\vec{\sigma}\cdot\vec{B} - i\vec{\alpha}\cdot\vec{E})\psi \quad . \tag{A14}$$

The square of the kinetic momentum four-vector is

$$\pi\cdot\pi = (p - \frac{e}{c}A)\cdot(p - \frac{e}{c}A)$$

$$= (p_o - \frac{e}{c}A_o)^2 - (\vec{p} - \frac{e}{c}\vec{A})^2$$

$$\pi\cdot\pi = (\frac{E}{c} - \frac{e}{c}\phi)^2 - (\vec{p} - \frac{e}{c}\vec{A})^2 \quad .$$

With this result, Eq. (A14) becomes

$$(E - e\phi)^2\psi = [c^2(\vec{p} - \frac{e}{c}\vec{A})^2 + (mc^2)^2 - ec\hbar(\vec{\sigma}\cdot\vec{B} - i\vec{\alpha}\cdot\vec{E})]\psi \quad . \tag{A15}$$

Equation (A15) is the desired second order equation for the four-component spinor ψ. It should be noted that if ψ is a solution to the

linear equation (A4), then it is also a solution to the quadratic equation (A15). As pointed out by Rose,[2] the presence of the non-hermitian term $i\vec{\alpha}\cdot\vec{E}$ in Eq. (A15) need not cause concern. Equation (A15) is not, strictly speaking, a quantum mechanical wave equation since it is not in the Hamiltonian form, i.e. instead of being written

$$\mathcal{H}\psi = i\hbar \frac{\partial}{\partial t}\psi$$

it contains the second time derivative $-\hbar \frac{\partial^2\psi}{\partial t^2} = E^2$.

B. Effective Fields of a TM_{010} Cylindrical Cavity

I. Introduction: This appendix contains detailed calculations which supplement the discussions of Chapters III and IV regarding the electric and magnetic fields experienced by an atomic beam as it traverses a cylindrical cavity that is resonating in the TM_{010} mode. Expressions are found which relate the fields and the magnetic vector potential to the measurable cavity parameters P, Q, ℓ and ν_o (defined below). Suitable spatial averages are made to deduce the effective fields which act on an atom when it passes along a diameter midway between the plane ends of the cavity.

II. Standing Wave Field Configuration: The explicit expressions for the electric and magnetic fields inside an evacuated, cylindrical cavity of radius R operating in the TM_{010} mode are,[1] in Gaussian units,

$$\vec{E} = \hat{z}\, E_0\, J_0\left(\frac{x_{01}}{R}\rho\right) e^{-i\omega t} \quad , \tag{B1}$$

and

$$\vec{B} = -\hat{\phi}\, iE_0\, J_1\left(\frac{x_{01}}{R}\rho\right) e^{-i\omega t} \quad . \tag{B2}$$

where $x_{01} = 2.405$ is the first root of the zeroth Bessel function $J_0(x)$

and ρ, ϕ and z are the radial, azimuthal, and axial coordinates, respectively, of a point inside the cavity referred to a cylindrical coordinate system whose origin lies at the center of one of the circular ends of the cavity.

The magnetic field lines are circles concentric with the cylinder axis, while the electric field lines are straight lines parallel to the cylinder axis.

Since no charges are present in the evacuated cavity, the electrostatic scalar potential vanishes and the electric field satisfies

$$\vec{E} = -\frac{1}{c}\frac{\partial \vec{A}}{\partial t} \quad .$$

Hence,

$$\vec{A} = -c \int \vec{E}\, dt = -z\, c\, E_0\, J_0 \left(\frac{x_{01}}{R}\rho\right) \int e^{-i\omega t}\, dt$$

or

$$\vec{A} = -\hat{z}\, i\frac{c}{\omega} E_0\, J_0 \left(\frac{x_{01}}{R}\rho\right) e^{-i\omega t} \quad . \tag{B3}$$

It can be verified by taking the curl of Eq. (B3) that Eq. (B2) satisfies

$$\nabla \times \vec{A} = \vec{B}$$

as it should

III. Field Amplitudes: It remains to express the amplitude E_0 in terms of the measurable cavity parameters P, Q, ℓ and ν_o. When this is done, one will be able to calculate the electric and magnetic fields and the vector potential at each point inside the cavity when P, Q, ℓ and ν_o are known, where

P = power input in erg/sec,

ℓ = length of cavity in cm,

ν_o = resonant frequency in sec^{-1},

and the parameter Q is defined by

$$Q \equiv \nu_o \frac{\text{Stored energy}}{\text{Power loss}} \quad . \tag{B4}$$

This parameter, Q, is sometimes referred to as the "unloaded Q"[2] since the only dissipation considered here is that which takes place within the cavity walls, namely ohmic heating. It should be pointed out that Q is directly related to the half power (or "3-db") points of the cavity power absorption curve, as measured when the cavity is used as a matched load. This resonance curve is of Lorentzian shape;[1] if the frequency separation between half-power points is $\Delta\nu$, then

$$Q = \frac{\nu_o}{\Delta\nu} \quad ,$$

where ν_o is the resonant frequency defined as the frequency at which maximum absorption occurs.

At equilibrium, the power dissipated by ohmic losses is equal to the input power P. If U is the time-averaged energy stored in the cavity, then, from Eq. (B4)

$$U = \frac{PQ}{\nu_o} \quad . \tag{B5}$$

The time average of the stored energy in an evacuated TM_{010} cavity is given by[1]

$$U = \frac{2\ell}{16\pi} \int_\sigma |E_z|^2 \, d\sigma$$

where ℓ is the length of the cavity and σ is the area of a cross section taken normal to the cavity axis. Thus,

$$U = \frac{|E_0|^2}{8\pi} \ell \int_0^{2\pi} d\phi \int_0^R \left[J_0 \left(\frac{x_{01}}{R} \rho \right) \right]^2 \rho \, d\rho \quad .$$

With the change of variables

$$r = \rho/R \quad ;$$

this becomes

$$U = \frac{|E_0|^2}{8\pi} 2\pi R^2 \ell \int_0^1 r J_0^2 (x_{01} r) \, dr \quad .$$

The integral appearing here is evaluated in standard integral tables:

$$\int_0^1 r J_0^2 (x_{01} r) \, dr = 1/2 \, J_1^2 (x_{01}) \quad .$$

Finally,

$$U = \frac{|E_0|^2}{8\pi} \pi R^2 \ell J_1^2 (x_{01}) \quad . \tag{B6}$$

Equations (B5) and (B6) can be combined to give the square of the amplitude E_0 in terms of P, Q, ℓ and ν_o. Thus

$$U = \frac{PQ}{\nu_o} = \frac{|E_0|^2}{8\pi} \pi R^2 \ell J_1^2 (x_{01}) \quad .$$

or

$$|E_0|^2 = \frac{8}{J_1^2 (x_{01})} \frac{PQ}{\nu_o \ell R^2} \quad . \tag{B7}$$

Now, the resonant frequency ν_o is related to the radius R by[1]

$$2\pi\nu_o = x_{01} \frac{c}{R} \quad ,$$

so that

$$R = \frac{x_{01}}{2\pi} \frac{c}{\nu_o} \tag{B8}$$

and Eq. (B7) becomes

$$|E_0|^2 = \frac{32\pi^2}{x_{01}^2 J_1^2(x_{01})} \frac{PQ\nu_o}{\ell c^2} \quad . \tag{B9}$$

When the numerical factors are collected, one obtains

$$|E_0|^2 = 203 \frac{PQ\nu_o}{\ell c^2} \quad . \tag{B10}$$

Eq. (B10) gives E_0 in statvolt/cm when P is in erg/sec, ν_o is in Hz and ℓ and c are in cgs units. An expression which may be used for practical calculations is

$$|E_0|^2 = 203 \frac{PQ\nu_o}{\ell} \tag{B11}$$

where now E_0 is in volt/cm when P is expressed in watts, ν_o in GHz, and ℓ in cm.

With E_0 given by Eq. (B10) one can obtain B in gauss and A in statvolts at any point within the cavity from Eqs. (B2) and (B3).

IV. Average Fields Acting on a Beam Atom: In this section a spatial average is taken of the quantities E^2, B^2 and A^2 to determine the effective fields experienced by atoms in a beam which travels along a cavity diameter midway between the ends. The average of the square of the magnetic field is taken, rather than of B itself, because it is B^2 which appears in expressions for transition probabilities and for the Bloch-Siegert Effect (Chapter IV, Sec. C). The average of the square of E is taken rather than of E itself because it is E^2 which

appears in expressions for the Stark Effect. The average of the square of A is taken rather than of A itself because it is A^2 which appears in the expression for the electron mass shift (Chapter II).

From Eqs. (B1), (B2) and (B3) one sees that the desired averages involve average values of squares of Bessel functions, i.e.,

$$\langle E^2 \rangle_\rho \propto \frac{1}{R}\int_0^R J_0^2\left(\frac{x_{01}}{R}\rho\right)\, d\rho$$

and

$$\langle B^2 \rangle_\rho \propto \frac{1}{R}\int_0^R J_1^2\left(\frac{x_{01}}{R}\rho\right)\, d\rho \quad .$$

These integrals are not evaluated in standard works on Bessel Functions, and it is necessary to evaluate them numerically. A Fortran II routine was written to perform the numerical integration. A subroutine evaluated $J_n(x)$ for a specified n and x to a chosen precision of about 0.1%. The main program employed the trapezoidal method to perform the integration. This method breaks up the area to be computed into m trapezoidal sections and adds their areas. The results for 100 intervals (m=100) are

$$\frac{1}{R}\int_0^R J_0^2\left(\frac{x_{01}}{R}\rho\right)\, d\rho = 0.478 \pm 0.002 \qquad \text{(B12)}$$

and

$$\frac{1}{R}\int_0^R J_1^2\left(\frac{x_{01}}{R}\rho\right)\, d\rho = 0.203 \pm 0.000 \qquad \text{(B13)}$$

The results for 200 intervals differed from these by .002 and .000, respectively, and this difference was chosen as the uncertainty in the calculation.

The one-dimensional averages just computed were made for a beam which has no height or width. The actual beam width is immaterial since neither B nor E (and hence A) depend upon axial position. Atoms traveling along a diameter go from $\rho = R$ to $\rho = 0$ and back to $\rho = R$. Due to the finite height of the beam, most atoms will travel along a chord parallel to the diameter, and hence their minimum radial position will be slightly greater than zero. The magnetic field is zero at $\rho = 0$. The average of B^2 for an off-diameter path (i.e., one which does not pass through $\rho = 0$) will be slightly larger than for a path that follows a diameter. The electric field and vector potential have their maxima at $\rho = 0$, so the average of E^2 and A^2 for an off-diameter path will be slightly smaller than for a path which follows a diameter.

If one were to average over the beam height, as well as along its length, one would obtain slightly different averages than those given by Eqs. (B12) and (B13). For example, consider an atom located on the upper or lower edge of the beam. It will pass through the cavity along a chord which passes to within a distance ℓ of the cavity axis (ρ=o), where 2ℓ is the vertical extent of the beam. The averages for such an atom are ($R = 1.546$ in., $\ell = .125$ in.)

$$\frac{1}{R-\ell} \int_{\ell}^{R} J_0^2 \left(\frac{x_{01}}{R} \rho\right) d\rho = 0.432 \pm .002 \qquad \text{(B14)}$$

$$\frac{1}{R-\ell} \int_{\ell}^{R} J_1^2 \left(\frac{x_{01}}{R} \rho\right) d\rho = 0.220 \pm .001 \ . \qquad \text{(B15)}$$

As anticipated, the average of J_1^2 (and hence of B^2) is slightly larger for an atom on the fringe of the beam than for an atom at the beam center, and the average of J_0^2 (and hence of E^2 and A^2) is slightly smaller for an atom on the edge of the beam than for one that follows a diameter. This difference amounts to about 10% in both cases.

Owing to the fact that there are deviations of unknown magnitude from the theoretical field configurations due to the holes cut in the cavity for entrance and exit apertures, and for the coupling loop, no averages will be exactly correct. Furthermore, uncertainties of about 5% arise in the determination of input power P and of Q, and these affect the accuracy to which the average fields can be determined. The following rough values will be used:

$$\langle J_0^2 \rangle_\rho = 0.455 \pm 0.023 \tag{B16}$$

$$\langle J_1^2 \rangle_\rho = 0.212 \pm 0.009 \quad . \tag{B17}$$

The uncertainties given here amount to about 5%.

In summary, the effective fields experienced by the beam will be taken to be

$$E = |E| e^{-i\omega t} \tag{B18}$$

$$B = i|B| e^{-i\omega t} \tag{B19}$$

$$A = -i|A| e^{-i\omega t} \tag{B20}$$

where

$$|E|^2 = 0.455\ E_0^2 \tag{B21}$$

$$|B|^2 = 0.212\ E_0^2 \tag{B22}$$

$$|A|^2 = 0.455 \left(\frac{c}{\omega}\right)^2 |E_0|^2 \qquad \text{(B23)}$$

and

$$|E_0|^2 = 203 \frac{PQ\nu_o}{\ell c^2} \qquad \text{(B10)}$$

with P given in erg/cm, ν_o in Hz, and ℓ and c in cgs units.

REFERENCES

Chapter I

I-[1] I. I. Rabi, S. Millman, P. Kusch, and J. R. Zacharias, The Molecular Beam Resonance Method for Measuring Nuclear Magnetic Moments, Phys. Rev. 55, 526 (1939).

I-[2] Paul A. Vanden Bout, Erol Aygun, Vernon J. Ehlers, Tuncay Incesu, Adnan Saplakoglu, and Howard A. Shugart, Precision Measurement of the Electronic g Factors of the Alkali Metals, Phys. Rev. 165, 88 (1968).

I-[3] R. D. Haun, Jr. and J. R. Zacharias, Stark Effect on Cesium-133 Hyperfine Structure, Phys. Rev. 107, 107 (1957).

I-[4] E. Lipworth and P. G. H. Sandars, Removal of Zeeman-Level Degeneracy in Alkali Atoms by an Electric Field, Phys. Rev. Letters 13, 716 (1964).

I-[5] M. C. Weiskopf, J. P. Carrico, H. Gould, E. Lipworth, and T. S. Stein, Electric Dipole Moment of the Cesium Atom. A New Upper Limit to the Electric Dipole Moment of the Electron, Phys. Rev. Letters 21, 1645 (1968).

I-[6] N. D. Sengupta, On the Scattering of Electromagnetic Waves by a Free Electron, Calcutta Mathematical Society Bulletin 44, 175 (1952).

I-[7] Edward S. Sarachik, Interaction of an Intense Laser Beam With a Free Electron, National Aeronautics and Space Administration Report NASA-TN-D5205 (unpublished), May 1969.

I-[8] Howard R. Reiss, A Proposed Experiment to Detect the Mass Shift of an Electron in an Intense Photon Field, Phys. Rev. Letters 17, 1162 (1966).

Chapter II

II-[1] Howard R. Reiss and Joseph H. Eberly, Green's Function in Intense-Field Electrodynamics, Phys. Rev. 151, 1058 (1966).

II-[2] Howard R. Reiss, Proposed Experiment to Detect the Mass Shift of an Electron in an Intense Photon Field, Phys. Rev. Letters 17, 1162 (1966).

II-[3] Hans A. Bethe and Edwin E. Salpeter, Quantum Mechanics of One and Two-Electron Atoms, Springer Verlag (1957) and Encyclopedia of Physics Vol. XXXV, Springer Verlag (1957).

II-[4] Leslie L. Foldy and Siegfried A. Wouthuysen, On the Dirac Theory of Spin 1/2 Particles and Its Non-Relativistic Limit, Phys. Rev. 78, 29 (1950).

II-[5] James D. Bjorken and Sidney D. Drell, Relativistic Quantum Mechanics, McGraw-Hill (1964), p. 51.

II-[6] Julian S. Schweber, Introduction to Relativistic Quantum Field Theory, Harper and Row (1961), p. 102.

II-[7] Norman F. Ramsey, Molecular Beams, Oxford (1955), Chapter II.

II-[8] R. Beehler, et al., An Intercomparison of Atomic Standards, IEEE Proceedings 54, 301 (1966).

II-[9] Richard G. Schlect and Douglas W. McColm, Hyperfine Structure of the Stable Lithium Isotope. I, Phys. Rev. 142, 11 (1966).

II-[10] Yau W. Chan, Victor W. Cohen, Max Lipsicas, and H. B. Silsbee, Nuclear Magnetic Moment and Hyperfine-Structure Anomaly of Na^{24}, Phys. Rev. 150, 933 (1966).

II-[11] H. Dahmen and S. Penselin, Measurement of the Nuclear Magnetic Dipole Moment of Au^{197} and Hyperfine Structure Measurements in

the Ground States of Au^{197}, Ag^{107}, Ag^{109} and K^{39}, Zeits Für Physik 200, 456 (1967).

II-[12] S. Penselin, T. Moran, V. W. Cohen, and G. Winkler, Hyperfine Structure of the Electronic Ground States of Rb^{85} and Rb^{87}, Phys. Rev. 127, 524 (1962).

II-[13] W. Markowitz, R. Glenn Hall, L. Essen, and J. V. L. Parry, Frequency of Cesium in Terms of Ephemeris Time, Phys. Rev. Letters 1, 105 (1958).

II-[14] Eugen Merzbacher, Quantum Mechanics, John Wiley & Sons (1961), p. 385.

II-[15] Norman F. Ramsey, A Molecular Beam Resonance Method with Separated Oscillatory Fields, Phys. Rev. 78, 695 (1950).

II-[16] Norman F. Ramsey, Resonance Transitions Induced by Perturbations at Two or More Different Frequencies, Phys. Rev. 100, 1191 (1955).

Chapter III

III-[1] G. Breit, The Isotope Displacement in Hyperfine Structure, Phys. Rev. 42, 348 (1932).

III-[2] H. Kopfermann, Nuclear Moments, Academic Press (1958), p. 136.

III-[3] N. F. Ramsey, Molecular Beams, Oxford (1955).

III-[4] Paul A. Vanden Bout, Vernon J. Ehlers, William A. Nierenberg, and Howard A. Shugart, Hyperfine-Structure Separations, Nuclear Magnetic Moments, and Hyperfine-Structure Anomalies of Gold-198 and Gold-199, Phys. Rev. 158, 1078 (1967).

III-[5] John D. Jackson, Classical Electrodynamics, John Wiley & Sons (1962), p. 254.

III-[6] Carol G. Montgomery (ed.), Technique of Microwave Measurements, Vol. I, Dover (1966), p. 302.

III-[7] Hugh D. Young, Statistical Treatment of Experimental Data, McGraw-Hill (paper, 1962), p. 124.

Chapter IV

IV-[1] N. F. Ramsey, Molecular Beams, Oxford (1955), p. 143.

IV-[2] Jon H. Shirley, Some Causes of Resonant Frequency Shifts in Atomic Beam Machines, I. Shifts Due to Other Frequencies of Excitation, National Bureau of Standards Report 7294, August 1962 (unpublished).

IV-[3] N. F. Ramsey, Resonance Transitions Induced by Perturbations at Two or More Different Frequencies, Phys. Rev. 100, 1191 (1955).

Appendix A

[1] James D. Bjorken and Sidney D. Drell, Relativistic Quantum Mechanics, McGraw-Hill (1964), Appendix A.

[2] M. E. Rose, Relativistic Electron Theory, John Wiley & Sons (1961), p. 123.

Appendix B

[1] John D. Jackson, Classical Electrodynamics, John Wiley & Sons (1962).

[2] Carol G. Montgomery (ed.), Technique of Microwave Measurements, Vol. I, Dover (1966), p. 288.

LEGAL NOTICE

TECHNICAL INFORMATION DIVISION
LAWRENCE RADIATION LABORATORY
UNIVERSITY OF CALIFORNIA
BERKELEY, CALIFORNIA 94720